FDTD MEASUREMENT OF THE REFLECTION COEFFICIENT ASSOCIATED WITH TOTAL INTERNAL REFLECTION FROM GAINY LORENTZIAN MEDIA

By

ABULIKEMU TUERXUNJIANG

Thesis submitted in partial fulfillment of the requirements for the degree of

MASTER OF SCIENCE IN PHYSICS

WASHINGTON STATE UNIVERSITY
Department of Physics and Astronomy

DECEMBER 2008

To the Faculty of Washington State University:

The members of the Committee appointed to examine the dissertation/thesis of A find it satisfactory and recommend that it be accepted.

_____
Chair

_____

_____

ACKNOWLEDGMENT

I would like to express my sincere appreciation and gratitude to my advisor Professor John B. Schneider for his constant assistance, support, and patient guidance. During research, not only did he teach me computational electro-dynamics, but also guided me how to be professional and mindful of details. His uncompromising quest for excellence and high-quality results encouraged me to work harder and to strive toward my goals.

I am also grateful to Professor Mark G. Kuzyk, who helped to steer my academic path when he was graduate student chair of the department. His initial suggestions that I study opto-electronics lead me, in the end, to this research project. I am also indebted to Professor Philip L. Marston, who agreed to serve on my committee. I admire his deep understanding of physics.

During the research process, I received invaluable help and assistance from my friends and colleagues, among whom I should note Lanchuan Zhou, who helped me to install Linux on the computer I subsequently used to complete this project. I am thankful to Santosh Swain, my roommate and good friend, who was a beacon of encouragement and provided me with spicy Indian foods almost every day.

FDTD MEASUREMENT OF THE REFLECTION COEFFICIENT ASSOCIATED WITH TOTAL INTERNAL REFLECTION FROM GAINY LORENTZIAN MEDIA

Abstract

by Abulikemu Tuerxunjiang
Washington State University
December 2008

Chair: John B. Schneider

The magnitude of the Fresnel reflection coefficient for total internal reflection (TIR) from a gainy medium has been a subject of controversy for over 40 years. We study the reflection coefficient from a half-space filled with a gainy or lossy Lorentzian medium using the finite-difference time-domain (FDTD) method. For comparison, a separate measurement is taken from a half space using the same configuration but with a medium of constant material parameters. The results show that the Fresnel reflection coefficient from a gainy half space is larger than unity upon TIR for incidence of above the critical angle and is smaller than unity for incidence below the critical angle. There is no difference in the reflection coefficients from a gainy (or lossy) Lorentzian half space with a gainy (or lossy) half space of constant coefficients. For reflection coefficient problems, materials with constant coefficients can be used to approximate a Lorentzian material at a single frequency.

LIST OF FIGURES

TABLE OF CONTENTS

Dedication

This thesis is dedicated to my mother Sa'et Khan Abdurashid and father Ablekim Rejep who provided strong emotional and financial support for my study in USA

CHAPTER 1
INTRODUCTION AND OVERVIEW

1.1 Introduction

The reflection of an electromagnetic wave from an interface between two dielectric media has been studied by researchers for a long time because of its relevance to a wide range of applications. Total internal reflection (TIR) will occur when an electromagnetic wave is incident upon the interface from a medium of higher refractive index to a medium of lower refractive index, provided that the incident angle is greater than the critical angle. The reflected energy could be amplified [1] or attenuated [2], depending on whether the medium of the lower refractive index is gainy (active or negative absorption) or lossy (passive or positive absorption). For simplicity, in many cases, the material parameters of the medium are approximated as constants. However, in reality, all materials, by their nature, have some form of frequency dependence of their permittivity and conductivity [3]. Therefore, the electromagnetic wave interaction with dispersive media is of significant importance because the modeling of dispersive materials is closer to reality.

We are interested in the magnitude of the reflection coefficient upon TIR from a Lorentzian gainy medium. Experimental and theoretical work on reflection problems have been concerned primarily with lossy materials [4-6], not gainy materials. On the other hand, reflection from gainy materials upon TIR has been studied since the 1960s, but most of that work was concerned with materials with constant parameters [7-15], not dispersive materials. Furthermore, there has been a lack of consistency in published experimental results as well as in theoretical explanations of the magnitude of the reflection coefficient upon TIR from a gainy medium of

constant material parameters. It is instructive to take a look at this controversy to understand the problem considered in this thesis.

In 1966, Koester observed amplification of the reflection coefficient at the interface between a lossless core of a fiber with a gainy cladding [1], which showed that the reflection coefficient could be greater than unity for TIR from a gainy medium. However, conventional optical theory predicts that the magnitude of the reflection coefficient is less than one for TIR regardless of whether the medium on the other side of the interface is gainy or lossy. To understand this, let us consider a region composed of two dielectric half spaces. As illustrated in Fig 1.1, the two half spaces are located on the left and right side of an interface. The half-space to the left of the interface is filled with medium 1 with dielectric constant ϵ_{r1} and conductivity σ_1. The half space to the right of the interface is filled with medium 2 with dielectric constant ϵ_{r2} and conductivity σ_2. To avoid reflection from the back edge of medium 2, we assume that medium 2 extends to infinity along the x direction. Both media are non-magnetic. Medium 1 is lossless so that $\sigma_1 = 0$ and medium 2 is either lossy if $\sigma_2 > 0$ or gainy if $\sigma_2 < 0$. In this project, we want to investigate the magnitude of the reflection coefficient from a Lorentzian gainy medium upon TIR, where the material parameters ϵ_{r2} and σ_2 of medium 2 are dependent on frequency. We require $\epsilon_{r2} < \epsilon_{r1}$ at the frequency of interest so that TIR can occur.

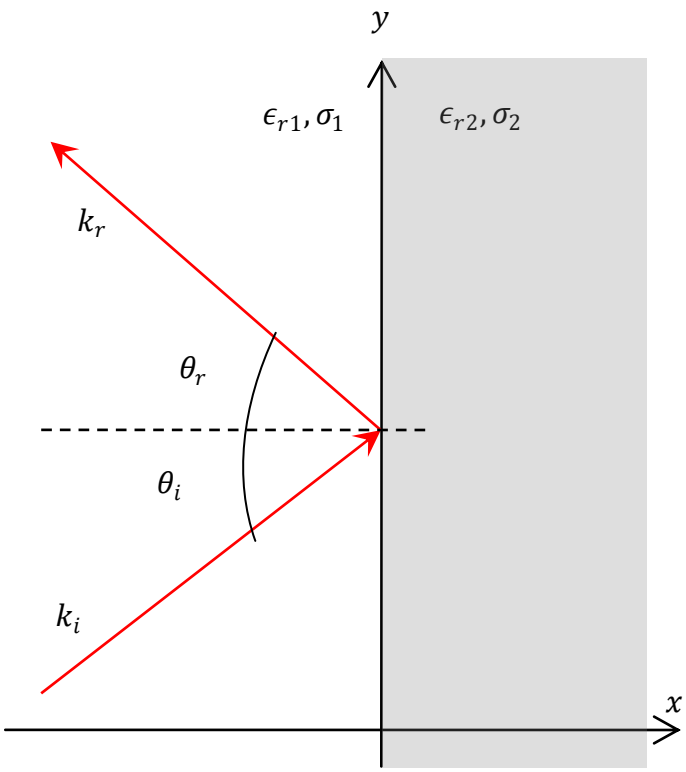

Figure 1. 1 System under consideration: dielectric half spaces.

Assume a plane wave of temporal dependence $\exp(j\omega t)$ is incident upon the interface from the left at the incident angle of θ_i with respect to the normal to the interface. The spatial dependence for the incident and reflected fields are given by $\exp(-j\mathbf{k}_i \cdot \mathbf{r})$ and $\exp(-j\mathbf{k}_r \cdot \mathbf{r})$, respectively, where $\mathbf{k}_i = (k_{ix}, k_{iy}) = (k_i \cos\theta_i, k_i \sin\theta_i)$. The reflected field wave vector differs from the incident wave vector only in the sign of the x-component so that $|\mathbf{k}_i| = |\mathbf{k}_r| = k_i = \omega\sqrt{\epsilon_{r1}\epsilon_0\mu_0}$. The spatial dependence of the field in medium 2 is given by $\exp((\mathbf{g} - j\mathbf{k}_t) \cdot \mathbf{r})$, where $\mathbf{k}_t = (k_{tx}, k_{ty})$, and $\mathbf{g}$ is the gain vector, the orientation of which corresponds to the direction of increasing amplitude and it has only an x-component. The tangential field across the interface must be continuous so that $k_{iy} = k_{ty}$.

The S-polarized Fresnel reflection coefficient can be expressed as:

$$R = \frac{k_i \cos\theta_i - (k_{tx} + jg_x)}{k_i \cos\theta_i + (k_{tx} + jg_x)}. \tag{1.1}$$

Alternatively, it can be written as [2]:

$$R = \frac{n_1 \cos\theta_i - (u_2 + jv_2)}{n_1 \cos\theta_i + (u_2 + jv_2)}, \tag{1.2}$$

where

$$2u_2^2 = n_2^2(1-\kappa_2^2) - n_1^2 \sin^2\theta_i + \sqrt{[n_2^2(1-\kappa_2^2) - n_1^2 \sin^2\theta_i]^2 + 4n_2^4\kappa_2^2}\,, \tag{1.3}$$

$$2v_2^2 = -n_2^2(1-\kappa_2^2) + n_1^2 \sin^2\theta_i + \sqrt{[n_2^2(1-\kappa_2^2) - n_1^2 \sin^2\theta_i]^2 + 4n_2^4\kappa_2^2}\,. \tag{1.4}$$

Here $n_1 = \sqrt{\epsilon_{r1}}$ and $n_2 = \sqrt{\epsilon_{r2}}$, which are the indices of refraction of medium 1 and medium 2, respectively. The κ_2 is related to the imaginary part of the complex index of refraction of medium 2, $\hat{n}_2$, as

$$\hat{n}_2 = n_2(1 + j\kappa_2) = \sqrt{\epsilon_{r2} - j\frac{\sigma_2}{\omega\epsilon_0}}, \tag{1.5}$$

or,

$$\kappa_2 = \frac{\mathrm{Im}(\hat{n}_2)}{n_2}. \tag{1.6}$$

As one can see in (1.3) and (1.4), κ_2 is squared everywhere it appears. A change in the sign of σ_2 only changes the sign of κ_2 in (1.5), which indicates that a sign change in σ_2 is not reflected in the expression of the Fresnel reflection coefficient in (1.2). Therefore, the sign of σ_2 does not affect the Fresnel reflection coefficient, i.e., the amplitude of the reflected wave is not amplified from a gainy interface. This contradicts with Koester's experimental observation, which showed the reflection coefficient could have a gain for TIR from a gainy medium [1].

Shortly after Koester's report of observing the gain in reflection from gainy medium, different interpretations were proposed to interpret the gain. Romanov and Shakhidzhanov

predicted that gain from a gainy medium occurs only for angles above the critical angle, where there will be a maximum amplified value at the critical angle [7]. Years later, Callary and Carniglia conclude that Romanov and Shakhidzhanov's theory is incorrect and showed reflectance is a continuous monotonic function of incident angle, greater than unity for all angles [9]. Several years later, Cybulski and Silverman showed that the reflection coefficients are greater than unity in the vicinity of the critical angle with a peak in the immediate vicinity and it falls towards unity as the incidence approaches 90 degrees [12]. More recently, Fan *et al.*, using a numerical method, showed that gain occurs beyond the critical angle [14]. Overall, research consistently agreed that gain is possible in reflections from a gainy medium upon TIR and the amount of gain is dependent on the incident angle. However, until recently experimental and theoretical results have been in discord in describing circumstances under which gain will occur and the amount of reflection.

In the most recent published research of 2008 [15], Willis *et al.* reformulated the Fresnel equation (1.1) by defining a new branch cut in the complex plain of g_x and k_{tx}, which explained the gain from a gainy medium upon TIR. Their numerical simulations supported their new branch cut theory and also confirmed the predictions of Romanov and Shakhidzhanov and Fan *et al*.

In Willis *et al.*'s work, the permittivity and the conductivity of the gainy medium is taken to be constant. However, as stated before, constant materials are inherently an approximation, e.g., it is impossible to have a lossless dielectric with constant permittivity. In reality, the material parameters can be a function of time, function of frequency, function of field intensity and/or function of direction.

In this thesis, we present an examination of the Fresnel reflection coefficient from a Lorentzian gainy or lossy medium, where the material parameters are dependent on frequency, using numerical simulations with the full-wave finite-difference time-domain (FDTD) method. We start by following Willis *et al.*'s approach [15] by modeling the interaction of a localized wave (Gaussian pulse) with a gainy half space of constant parameters. However some implementation details differ as will be described. Later, the gainy half space is replaced with a Lorentzian half space. In the end, the calculated reflection coefficients from a constant and Lorenzian gainy (or lossy) medium as well as the analytic solutions are compared.

The main contribution of this project is that we investigate the reflection coefficient from a Lorentzian gainy (or lossy) medium upon TIR and show that it closely agrees with the results obtained from constant gainy medium. We confirm that Willis *et al.*'s interpretation of the Fresnel's reflection equation with the new branch cut can be applied to the Lorentzian gainy materials as well.

1.2 General Overview of the Contents

Chapter 2 provides a brief overview of Maxwell's equations and the fundamental concepts of the FDTD method. Yee's algorithm, the stability of the FDTD system, the total-field/scattered-field boundary, and the perfectly matched layer will be discussed. Chapter 3 discusses the space-time profiles of a Gaussian beam formulation and numerical simulations. Technical problems like simulating oblique incidence of the Gaussian beam upon the interface and limiting the size of the transverse distance of the beam are considered. Chapter 4 provides an introduction to Lorentzian materials and discusses the implementation of the Lorentzian gainy materials in the FDTD method. In Chapter 5, a brief introduction is given for evanescent waves and the details of modeling the system including the configuration of the FDFD grid, material parameters,

Gaussian wave implementation and measurement of the reflection coefficients are discussed. The analytical and numerical results are compared and analyzed. Finally, a conclusion of the project is provided.

CHAPTER 2
INTRODUCTION TO THE FINITE-DIFFERENCE-TIME-DOMAIN METHOD

2.1 Brief Overview of Maxwell Equations

The time-dependent Maxwell's curl equations in a linear, isotropic, non-dispersive, lossy medium are given by

$$\nabla \times \boldsymbol{E} = -\mu \frac{\partial \boldsymbol{H}}{\partial t} - \sigma_m \boldsymbol{H} \,, \tag{2.1}$$

$$\nabla \times \boldsymbol{H} = \epsilon \frac{\partial \boldsymbol{E}}{\partial t} + \sigma \boldsymbol{E} \,, \tag{2.2}$$

where $\boldsymbol{E}$ is the electric field, $\boldsymbol{H}$ is the magnetic field, ϵ is the electrical permittivity, μ is the magnetic permeability, σ is the electric conductivity, and σ_m is the magnetic conductivity. The electrical permittivity ϵ and the magnetic permeability μ are often expressed in terms of relative permittivity ϵ_r and relative permeability μ_r, respectively, as

$$\epsilon = \epsilon_r \epsilon_0 \,, \tag{2.3}$$

$$\mu = \mu_r \mu_0 \,, \tag{2.4}$$

where ϵ_0 is the permittivity of free space of 8.854×10^{-12} F/m, and μ_0 is the permeability of free space of $4\pi \times 10^{-7}$ H/m.

The three-dimensional curl equations of (2.1) and (2.2) involve six different field components which are, in Cartesian coordinates, E_x, E_y, E_z, H_x, H_y, and H_z. In two-dimensional problems, we usually choose between one of two groups of three components each: (1) transverse magnetic fields (TMz) which consists of E_z, H_x, and H_y or (2) transverse electric fields (TEz) which consists of E_x, E_y, and H_z. In this project, we work with TMz fields. For TMz fields, the scalar equations obtained from (2.1) and (2.2) are

$$\frac{\partial E_z}{\partial t} = \frac{1}{\epsilon}\left[\frac{\partial H_y}{\partial x} - \frac{\partial H_x}{\partial y} - \sigma E_z\right], \tag{2.5}$$

$$\frac{\partial H_x}{\partial t} = \frac{1}{\mu}\left[-\frac{\partial E_z}{\partial y} - \sigma_m H_x\right], \tag{2.6}$$

$$\frac{\partial H_y}{\partial t} = \frac{1}{\mu}\left[\frac{\partial E_z}{\partial x} - \sigma_m H_y\right]. \tag{2.7}$$

2.2 The FDTD Method

2.2.1 Introduction

The finite-difference time-domain (FDTD) method is a powerful yet simple algorithm to solve Maxwell's equations in the time-domain. Since it is a time-domain method, solutions can cover a wide frequency range with a single simulation. The FDTD algorithm was introduced by Yee in 1966 [16], but due to the limited capabilities of computers at that time, it did not get much attention. Since about 1990 when high-speed computers became more widely available, FDTD techniques have emerged as one of the primary means to model many scientific and engineering problems dealing with electromagnetic fields.

The FDTD method employs finite differences as approximations to both the spatial and temporal derivatives that appear in Maxwell's curl equations. In finite difference techniques the first-order derivative of a function $f(x)$ at a point x_0 with an offset of $\pm\frac{\Delta_x}{2}$ will be expressed as

$$f'(x_0) \cong \frac{f\left(x_0 + \frac{\Delta_x}{2}\right) - f\left(x_0 - \frac{\Delta_x}{2}\right)}{\Delta_x}, \tag{2.8}$$

where the error introduced by the approach is of the order of Δ_x^2.

2.2.2 Yee Algorithm

The Yee FDTD algorithm can be summarized as [17]:

- Replace all the derivatives in Ampere's and Faraday's laws with finite differences. Discretize space and time so that the electric and magnetic fields are staggered in both space and time.
- Solve the resulting difference equations to obtain "update equations" that express the (unknown) future fields in terms of (known) past fields.
- Initialize the fields to some known state(usually zero).
- Introduce energy to the computational domain via a suitable method.
- Evaluate the magnetic fields one time-step into the future so they are now known (effectively they become past fields).
- Evaluate the electric fields one time-step into the future so they are now known (effectively they become past fields).
- Repeat the previous three steps until the fields have been obtained over the desired duration.

Thus, the basic idea of the FDTD algorithm is that the time-dependent Maxwell's curl equations are discretized using central-difference approximations to the space and time partial derivatives. The resulting finite-difference equations are computed in a leapfrog manner so that the electric field vector components in space are solved at a given instant in time and the magnetic field vector components are solved at the next instant in time. The process is repeated over and over again until the field has achieved a desired state (e.g., gone to zero).

In order to use the FDTD method, a computational domain must be established and space and time need to be discretized. The computational domain corresponds to the physical region over which the simulation will be performed. In the 2D case, the computational domain is

discretized by $M \times N$ sample points, also known as nodes, where M is the number of points in the x direction and N is the number of points in the y direction. The $\boldsymbol{E}$ and $\boldsymbol{H}$ fields are determined at every node in space within that computational domain. The location of a node within the computational domain is given by

$$(x, y) = \left(m\Delta_x, n\Delta_y\right). \tag{2.9}$$

Here, Δ_x and Δ_y are the spatial offsets between sample points in the x and y direction, respectively. The indices m and n correspond to the spatial location in the x and y direction, respectively. Further, we denote any function $U(x, y, t)$ of space and time evaluated at a discrete point in the grid and a discrete point in time as

$$U(x, y, t) = U\left(m\Delta_x, n\Delta_y, q\Delta_t\right) = U^q[m, n], \tag{2.10}$$

where the index q is an index that corresponds to the temporal step and Δ_t is the temporal step size.

Following the notation described in (2.9) and (2.10), each of the field components for TMz polarization are expressed as

$$H_x(x, y, t) = H_x\left(m\Delta_x, n\Delta_y, q\Delta_t\right) = H_x^q[m, n], \tag{2.11}$$

$$H_y(x, y, t) = H_y\left(m\Delta_x, n\Delta_y, q\Delta_t\right) = H_y^q[m, n], \tag{2.12}$$

$$E_z(x, y, t) = E_z\left(m\Delta_x, n\Delta_y, q\Delta_t\right) = E_z^q[m, n]\ . \tag{2.13}$$

In the Yee algorithm for TMz polarization, the spatial arrangement of electric and magnetic field nodes is shown in Fig 2.1. The electric-field nodes are shown as circles and the magnetic-field nodes as squares with a line that indicates the orientation of the field component. One can see that the electric and magnetic field components are arranged in such a way that the

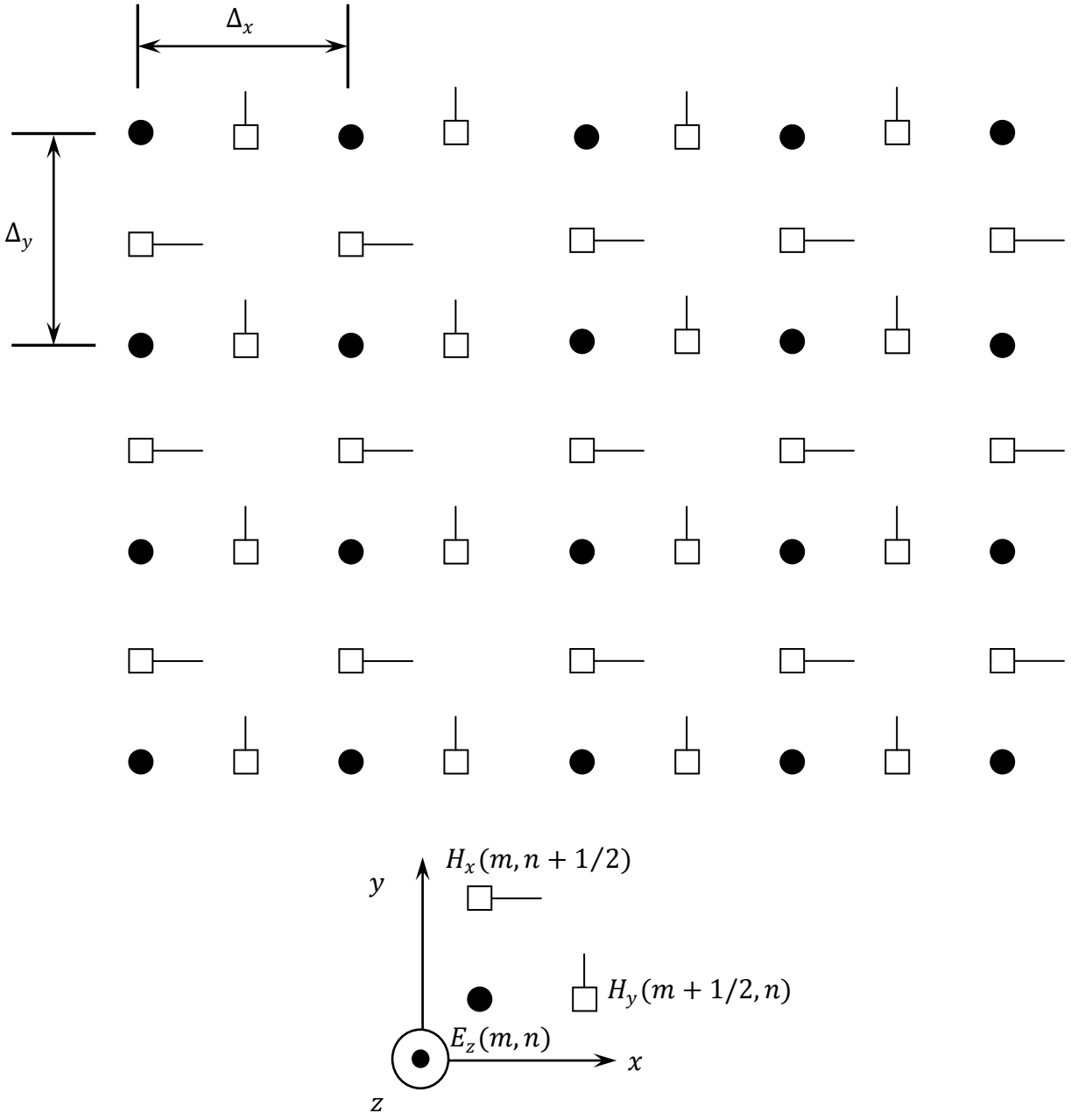

Figure 2. 1 Spatial arrangement of electric and magnetic field nodes for TMz polarization.

electric field nodes fall at integer spatial steps and the magnetic field nodes are offset a half spatial step in either the x or y direction. The electric field is assumed to exist at integer multiples of the temporal step while both magnetic field components are offset a half time-step from the electric fields. The diagram at the bottom of the figure indicates nodes with their offsets

given explicitly in the spatial arguments. The grid starts with electric field nodes and ends with electric field nodes so that at the top of the grid the computational domain lacks an H_x node and at the right edge lacks an H_y node. When we say the dimensions of the TMz computational domain are $M \times N$ nodes, it indicates that there are $M \times N$ nodes of E_z, $M \times (N-1)$ nodes of H_x, and $(M-1) \times N$ nodes of H_y.

With the above arrangement of nodes in the computational domain, the finite difference approximation of (2.5) expanded about space-time point $(m\Delta_x, n\Delta_y, (q+1/2)\Delta_t)$ is

$$\frac{E_z^{q+1}[m,n] - E_z^q[m,n]}{\Delta_t} = \frac{1}{\epsilon}\left(\frac{H_y^{q+1/2}\left[m+\frac{1}{2},n\right] - H_y^{q+1/2}\left[m-\frac{1}{2},n\right]}{\Delta_x} - \frac{H_x^{q+1/2}\left[m,n+\frac{1}{2}\right] - H_x^{q+1/2}\left[m,n-\frac{1}{2}\right]}{\Delta_y} - \sigma\frac{E_z^{q+1}[m,n] + E_z^q[m,n]}{2}\right). \tag{2.14}$$

Here, the E_z value at time step $q+1/2$ that appears in the conduction current term is approximated by the arithmetic average of the past value of E_z at time step q and, the future value of E_z at time step $q+1$. Solving (2.14) for the future value $E_z^{q+1}[m,n]$ yields:

$$E_z^{q+1}[m,n] = \frac{1-\frac{\sigma\Delta_t}{2\epsilon}}{1+\frac{\sigma\Delta_t}{2\epsilon}}E_z^q[m,n] + \frac{1}{1+\frac{\sigma\Delta_t}{2\epsilon}}\left(\frac{\Delta_t}{\epsilon\Delta_x}\left\{H_y^{q+1/2}\left[m+\frac{1}{2},n\right] - H_y^{q+1/2}\left[m-\frac{1}{2},n\right]\right\} - \frac{\Delta_t}{\epsilon\Delta_y}\left\{H_x^{q+1/2}\left[m,n+\frac{1}{2}\right] - H_x^{q+1/2}\left[m,n-\frac{1}{2}\right]\right\}\right). \tag{2.15}$$

The material parameters ϵ and σ will be specified at every node of the FDTD grid. Equation (2.15) is known as the update equation for the E_z field. It shows that the future value of E_z can be obtained by its past value and the neighboring magnetic field components.

Similarly, we can derive finite-difference expressions based on Yee's algorithm for the H_x and H_y field components given by Maxwell's equations (2.6) and (2.7). Expanding (2.6) about the space-time point $\left(m\Delta_{\mathrm{x}}, (n+1/2)\Delta_y, q\Delta_t\right)$, the resulting update equation for H_x is

$$H_x^{q+\frac{1}{2}}\left[m, n+\frac{1}{2}\right] = \frac{1-\frac{\sigma_m \Delta_t}{2\mu}}{1+\frac{\sigma_m \Delta_t}{2\mu}} H_x^{q-\frac{1}{2}}\left[m, n+\frac{1}{2}\right] - \frac{1}{1+\frac{\sigma_m \Delta_t}{2\mu}} \frac{\Delta_t}{\mu \Delta_{\mathrm{y}}} \left(E_z^q[m, n+1] - E_z^q[m, n]\right). \tag{2.16}$$

Expanding (2.7) about the space-time point $\left((m+1/2)\Delta_{\mathrm{x}}, n\Delta_y, q\Delta_t\right)$, the resulting update equation for H_y is

$$H_y^{q+\frac{1}{2}}\left[m+\frac{1}{2}, n\right] = \frac{1-\frac{\sigma_m \Delta_t}{2\mu}}{1+\frac{\sigma_m \Delta_t}{2\mu}} H_y^{q-\frac{1}{2}}\left[m+\frac{1}{2}, n\right] + \frac{1}{1+\frac{\sigma_m \Delta_t}{2\mu}} \frac{\Delta_t}{\mu \Delta_{\mathrm{x}}} \left(E_z^q[m+1, n] - E_z^q[m, n]\right). \tag{2.17}$$

The material parameters μ and σ_m will be specified at every node of the FDTD grid both in (2.16) and (2.17). In FDTD simulations, there is no requirement that the respective spatial step sizes Δ_{x} and Δ_{y} be equal. However, in this project, the grid is set to be uniform so that $\Delta_x = \Delta_y = \delta$.

By applying the system of update equations (2.15), (2.16), and (2.17) to every node in the grid, the electric and magnetic field components can be obtained at each time step. By repeating

the procedure, a desired electromagnetic field can be computed. Similar systems of update equations can be derived for 1D and 3D problems [17-20].

2.2.3 Stability of the system

While defining a FDTD model for a given problem, one has to choose proper grid parameters such that the spatial increment Δ_x and Δ_y are small enough to resolve a structure's geometrical details and/or the shortest wavelength of the spectrum propagating in the grid. Once the spatial increment is chosen, the temporal increment Δ_t is bounded via a stability condition [21]:

$$\Delta_t \leq \frac{1}{c\sqrt{\frac{1}{\Delta_x^2}+\frac{1}{\Delta_y^2}}}, \tag{2.18}$$

where c is the speed of light in free space. For a uniform grid of $\Delta_x = \Delta_y = \delta$, the bound simplifies to

$$\Delta_t \leq \frac{\delta}{c\sqrt{2}}. \tag{2.19}$$

For uniform grids, in other dimension, the upper bound is given by

$$\Delta_t \leq \frac{\delta}{c\sqrt{D}}, \tag{2.20}$$

or

$$\frac{c\Delta_t}{\delta} \leq \frac{1}{\sqrt{D}}, \tag{2.21}$$

where D denotes the dimension (that can be either 1, 2, or 3). In FDTD simulations, we usually define the constant [22]

$$S_c = \frac{c\Delta_t}{\delta}, \tag{2.22}$$

where S_c is called the Courant number. It is often convenient to set S_c for the system rather than setting the values of δ and/or Δ_t separately.

2.3.4 Excitation of the grid: total-field/scattered-field boundary

The FDTD grid needs to be excited by a source to introduce an electromagnetic field. There are many case-dependent source implementations available, the simplest of which is hard-wiring the source. In this implementation, some field components at some locations are given pre-defined values in the time-domain, while the other field values are updated normally. The weakness of the hard source is that any wave incident on the source will be reflected. To make the source "transparent," the system can be excited using an additive source term [21]. The weakness of an additive source is that it propagates in all directions, which can make it hard to separate the incident field from the reflected field or scattered field. Our goal is to construct a source such that the excitation only propagates to one side of a boundary. We will accomplish this using what is known as a total-field/scattered-field (TF/SF) boundary.

The total-field scattered-field (TF/SF) formulation is a method for introducing energy into the FDTD grid [23-25]. It defines a boundary, identified as the TF/SF boundary, which divides the computational domain into two regions: a total-field (TF) region which contains both the incident field and any scattered field, and a scattered-field (SF) region which contains only scattered fields. Figure 2.2 shows a TMz grid with a rectangular boundary, where the TF region is enclosed within the TF/SF boundary which is drawn with a dashed line. The SF region is any portion of the grid that is outside this boundary. Nodes that have a neighbor on the other side of the boundary are enclosed in a solid rectangle with rounded corners, where these encircled nodes are tangential to the TFSF boundary.

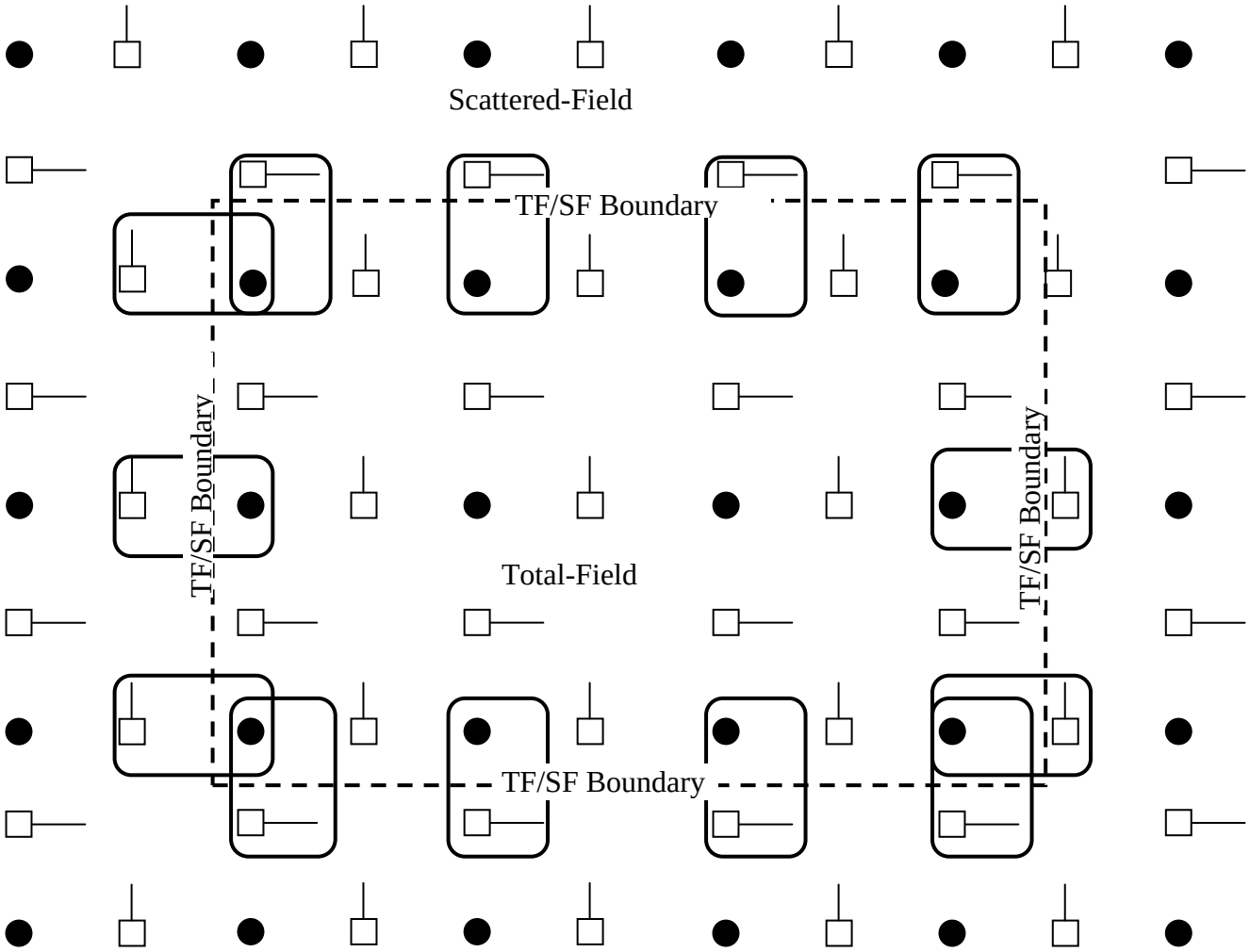

Figure 2. 2 Depiction of a total-field/scattered-field boundary in a TMz grid.

To implement the TF/SF method, one must know the incident field at every node which has a neighbor on the other side of the TFSF boundary. The incident field must be known at all these nodes and for every time-step. For this project, an auxiliary FDTD grid will be implemented to model the propagation of the incident wave, where we call the original FDTD grid the main grid to avoid confusion. The auxiliary grid is assumed to be filled with a homogenous medium and uses the same Courant number as the main grid, but is otherwise completely separate from the main grid. The source will be hard-wired to nodes on one side of the auxiliary grid. The other sides of the auxiliary grid must be suitably terminated so that the

incident field does not reflect back from its boundaries. In the main grid, for nodes which are tangential to the TFSF boundary and have a neighboring node on the other side of the boundary that requires the knowledge of incident field, the values of the field will be obtained from the corresponding nodes from the auxiliary grid. These nodes must have their update-equations corrected to account for the existence of the TFSF boundary. For the update of a node which is in the TF region and depends on a neighboring node in the SF region, the incident field is added to that neighboring node. Conversely, for the update of a node which is in the SF region and depends on a neighboring node in TF region, the incident field is subtracted from that neighboring node. A detailed description of the implementation of the TF/SF boundary technique can be found in [26-28].

2.4 Terminating the Grid: Perfectly Matched Layers

In most of the problems using FDTD simulations, the FDTD grid is terminated using suitable absorbing boundary conditions (ABC) so that no field reflects back from the edge of the computational domain (or the reflected field is trivially small). With a suitable ABC applied to the edge of the grid, the computational domain behaves as if it were infinite even though there are a finite number of nodes in the grid. A number of analytical techniques have been introduced to achieve this goal, e.g., the Bayliss-Turkel ABC [29], Engquist-Majda operator and Mur ABC [30][24], Trefethen-Halpern ABC [31], Higdon ABC [32], Liao extrapolation [33], Mei-Fang superabsorption [34], and Ramahi complementary operators [35][36]. Although these ABC's are useful in some FDTD simulations, for many problems they are not sufficiently accurate, introducing a 0.5% to 5% reflection. An alternate approach is the perfectly matched layer (PML), which is a highly effective ABC technique first proposed by Bérenger in 1994 [37].

The approach used in the PML technique is to terminate the outer boundaries of the FDTD grid with a lossy medium. Ideally, the lossy medium is only a few cells thick, reflectionless to all impinging waves over their full frequency spectrum, highly absorbing and effective in the near field of a source or scatterer. In the original work of Bérenger, which is called split-field PML, fields in the PML are split into two separate parts, and the actual field components are the sum of these two parts. By splitting the field, a virtual anisotropic medium is created with the necessary phase velocity and conductivity to eliminate reflections at an interface between a PML and non-PML region. There is no loss in the direction tangential to the interface but there is loss normal to the interface.

In the 2D TMz case, the equations governing the PML are [38]:

$$j\omega\mu_2 H_y + \sigma_{mx} H_y = \frac{\partial E_z}{\partial x}, \tag{2.23}$$

$$j\omega\mu_2 H_x + \sigma_{my} H_x = -\frac{\partial E_z}{\partial y}, \tag{2.24}$$

$$j\omega\epsilon_2 E_{zx} + \sigma_x E_{zx} = \frac{\partial H_y}{\partial x}, \tag{2.25}$$

$$j\omega\epsilon_2 E_{zy} + \sigma_y E_{zy} = -\frac{\partial H_x}{\partial y}, \tag{2.26}$$

where ϵ_2 and μ_2 are the permittivity and the permeability of the lossy medium, σ_{mx} and σ_{my} are the magnetic conductivities associated not with the x and y components of the magnetic field, but rather with propagation in the x or y direction in the lossy anisotropic medium. As one can see from (2.25) and (2.26), the E_z component has been split into two parts E_{zx} and E_{zy}, where the actual field is the sum of the two parts such that $E_z = E_{zx} + E_{zy}$. One can also see that there are two electrical conductivities: σ_x and σ_y, which can be chosen independently. If they were constrained to be equal, equations (2.25) and (2.26) could be merged, resulting in the ordinary

Maxwell's equations (2.5). A PML can conveniently be parameterized by the set of conductivities ($\sigma_x, \sigma_{mx}, \sigma_y, \sigma_{my}$). The parameters of a PML region and the material parameters of the adjacent non-PML region must satisfy certain matching conditions [39] in order to eliminate reflections. For example, consider a PML region which is separated from a non-PML region at a boundary of $x = 0$, where the incident wave impinges upon the boundary at the arbitrary angle θ relative to the x axis. The TMz polarized wave is incident from the non-PML region, which is to the left of the boundary, onto the PML region, which is to the right of the boundary. Then the matching conditions are given by

$$\epsilon_2 = \epsilon_1 , \tag{2.27}$$

$$\mu_2 = \mu_1 , \tag{2.28}$$

$$\sigma_y = \sigma_{my} = 0 , \tag{2.29}$$

$$\frac{\sigma_x}{\epsilon_2} = \frac{\sigma_{mx}}{\mu_2}, \tag{2.30}$$

where ϵ_1 and μ_1 are the permittivity and the permeability of non-PML region. Under these matching conditions, equations (2.23)-(2.26) dictate implementation within the FDTD method.

In addition to the split-field PML formulation discussed above, there are other PML formulations, in which a complex coordinate-stretching technique [40][41] is used. This technique constructs the PML from an anisotropic, dispersive material and it does not require the fields to be split. The split-field equations are reformulated in a non-split form that maps Maxwell's equations into a complex coordinate system. To do this, we define

$$S_w = 1 + \frac{\sigma_w}{j\omega\epsilon_2}, \tag{2.31}$$

where the subscript w is either x or y. Employing the matching relations (2.27)-(2.30), the governing equations of split-field PML (2.23)-(2.25) can be re-written as

$$j\omega\mu_2 H_y = \frac{1}{S_x}\frac{\partial E_z}{\partial x}, \tag{2.32}$$

$$j\omega\mu_2 H_x = -\frac{1}{S_y}\frac{\partial E_z}{\partial y}, \tag{2.33}$$

$$j\omega\epsilon_2 E_z = \frac{1}{S_x}\frac{\partial H_y}{\partial x} - \frac{1}{S_y}\frac{\partial H_x}{\partial y}, \tag{2.34}$$

where, (2.34) is derived by adding (2.25) and (2.26). If we define a new operator $\widetilde{\nabla}$ in the 3D space as

$$\widetilde{\nabla} = \hat{\mathbf{a}}_x \frac{1}{S_x}\frac{\partial}{\partial x} + \hat{\mathbf{a}}_y \frac{1}{S_y}\frac{\partial}{\partial y} + \hat{\mathbf{a}}_z \frac{1}{S_z}\frac{\partial}{\partial z}, \tag{2.35}$$

Maxwell's curl equations become

$$j\omega\epsilon_2 \mathbf{E} = \widetilde{\nabla} \times \mathbf{H}, \tag{2.36}$$

$$-j\omega\mu_2 \mathbf{H} = \widetilde{\nabla} \times \mathbf{E}. \tag{2.37}$$

This is known as the stretched-coordinate PML formulation since, as shown in (2.35), the complex S terms scale the various coordinate directions. Additionally, there is no explicit mention of split fields in this formulation. These equations are implemented in the FDTD algorithm with the help of convolution. A more efficient implementation was published by Roden and Gedney [42] that is based on the stretched-coordinate form of the PML. This formulation is known as convolutional PML (CPML) and is used in this project. The details of implementing a PML in the FDTD method can be found in [38][39].

CHAPTER 3
PULSED GAUSSIAN BEAM

3.1 Introduction

A pulsed Gaussian beam is used to excite the FDTD grid in this project. A Gaussian beam is electromagnetic radiation where the transverse electric field and intensity distributions are described by Gaussian functions. Gaussian beams are usually considered in situations where the beam divergence is relatively small, so that the paraxial approximation can be applied.

3.2 Mathematical Formulation and Beam Parameters

Consider a Gaussian beam propagating in a homogeneous medium. If the propagation direction is assumed to be along the z axis (which is also the beam axis) and r denotes the transverse distance from the beam axis, as shown in Fig. 3.1, the frequency domain (FD) representation of the beam can be written as [43][44]:

$$U(r,z,\omega) = \tilde{A}(\omega)\frac{w_0}{w(z)}\exp\left\{-jk\left[z+\frac{r^2}{2q(z)}\right]+j\varphi(z)\right\}, \tag{3.1}$$

where $U(r,z,\omega)$ is the complex electric field amplitude of the beam, $\tilde{A}(\omega)$ is the spectral amplitude of the pulse, $k=\frac{2\pi}{\lambda}$ is the wave number, and λ is the wavelength. The other parameters are given by

$$\frac{1}{q(z)} = \frac{1}{R(z)} - j\frac{2}{k_0 w^2(z)}, \tag{3.2}$$

$$w^2(z) = {w_0}^2\left[1+\left(\frac{z}{z_0}\right)^2\right], \tag{3.3}$$

$$R(z) = z\left[1 + \left(\frac{z_0}{z}\right)^2\right], \tag{3.4}$$

$$\varphi(z) = \tan^{-1}\left(\frac{z}{z_0}\right), \tag{3.5}$$

$$z_0 = \frac{\pi w_0^2}{\lambda_0}, \tag{3.6}$$

where w_0 is the waist size of the beam, k_0 and λ_0 are the wavenumber and wavelength, respectively, at the peak frequency. The peak frequency is the frequency with the greatest spectral content. The functions $R(z)$, $w(z)$ and $\varphi(z)$ need special attention and will be described in detail.

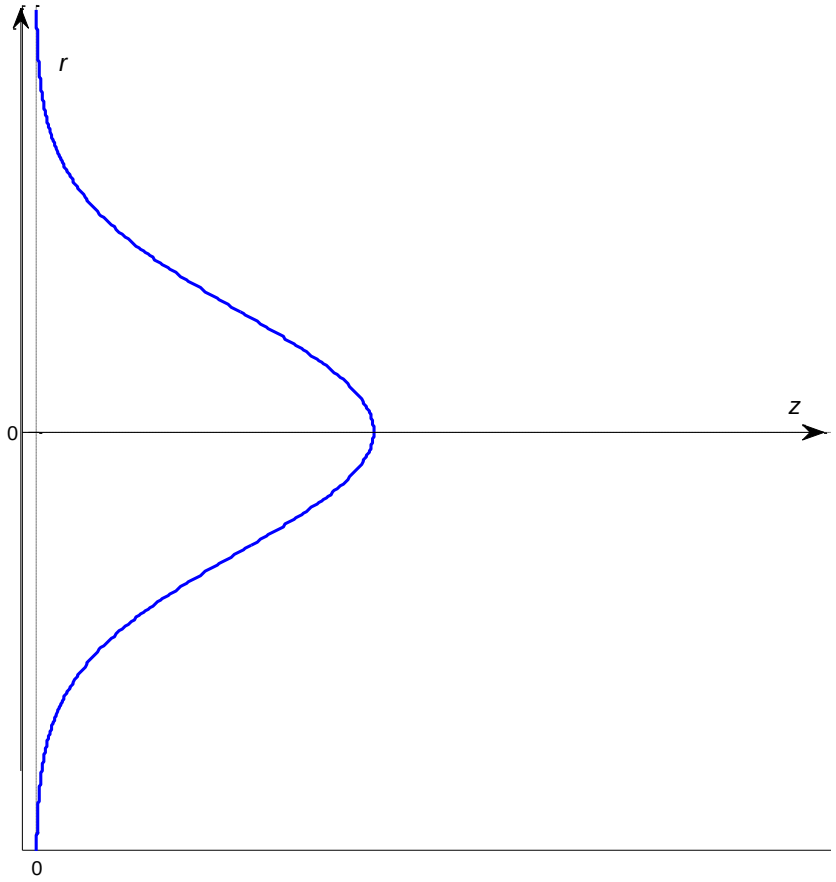

Figure 3. 1 Beam profile of a propagating Gaussian beam.

Here it should be noted that there are a typo in Wang *et al.*'s paper [43] where $\frac{1}{q(z)}$ is mistyped as $q(z)$ in the corresponding equation (3) of the paper.

3.2.1 Beam parameters

When a Gaussian beam propagates in a homogeneous medium, the intensity profile will change during propagation. The intensity (proportional to the square of the electric field) is symmetric about the beam axis and varies as [45]:

$$I = |U(r, z, \omega)|^2 \propto \exp\left(\frac{-2r^2}{w^2(z)}\right), \tag{3.7}$$

where r is the perpendicular distance from the beam axis, and $w(z)$ is the beam waist which is defined in (3.3). The parameter $w(z)$ describes the variation of the beam profile along the axis of the beam and it has a minimum value w_o when $z = 0$; This minimum value w_o is defined as waist size of the beam, while we call $w(z)$ the beam waist.

The beam waist $w(z)$ (as opposed to the waist size w_o) corresponds to the transverse distance from the axis to the point where the intensity has fallen to $1/e^2$ of the intensity on the axis, or correspondingly, where the electric field has dropped by $1/e$. Note that the beam waist is defined as a distance in the transverse direction, but is a function of z. For a given z, 86.5% of the energy is contained within a beam radius of $r = w(z)$. At $r = 2w(z)$, or twice the beam waist, the intensity is 0.0003 of its value on the axis. The power contained within a radius r has a profile similar to the intensity, and can be obtained by integrating the intensity distribution from 0 to r.Figure 3.2 shows the intensity distribution of the Gaussian beam. The length $z_0 = \frac{\pi\sigma_0^2}{\lambda_0}$ which appeared in (3.3) - (3.6) is known as the Rayleigh length, which is the length the beam can

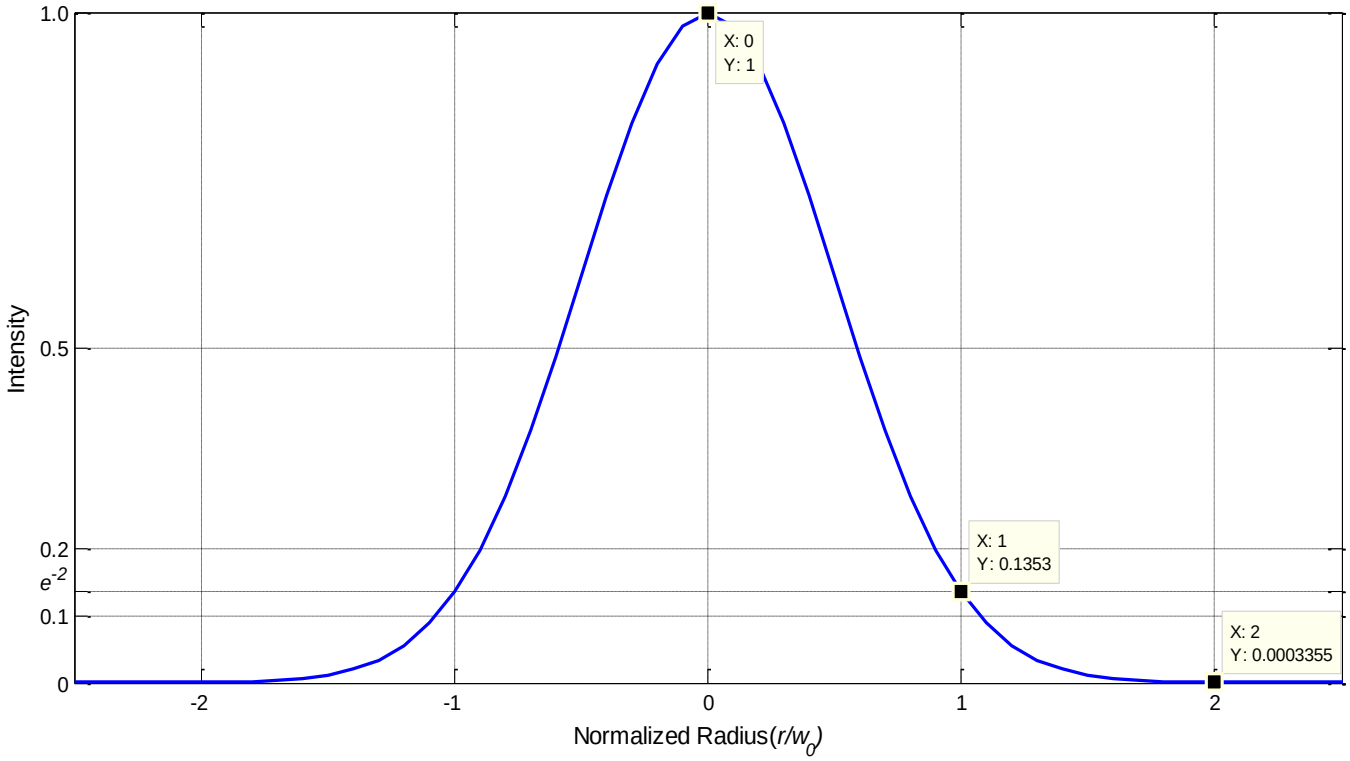

Figure 3. 2 The intensity distribution of a Gaussian beam.

propagate without significantly diverging. By propagating a Rayleigh length z_0 from $z = 0$, the beam waist expands from w_0 to $\sqrt{2}w_0$.

Another important parameter that describes the Gaussian beam propagation is $R(z)$, which is known as the radius of curvature of the wavefront of the Gaussian beam and is given by (3.4). When z tends to infinity, $R(z)$ shows a linear variation with z that is typical of a spherical wavefront that originated at z = 0; i.e., coming from a point source. However, the radius of curvature is infinite at $z = 0$. This means that at the minimum beam waist the wavefront is plane. A detailed description of the beam curvature is shown in Fig. 3.3, where the z coordinate is the propagation distance normalized to z_0. From Fig. 3.3 one can see that the beam has a minimum beam waist w_0 that occurs at $z = 0$ and it gradually expands to either side of $z = 0$. The expanding beam has a curved wavefront with a radius of curvature $R(z)$. The beam angular spread at a propagation distance z is called the divergence of the beam and given by

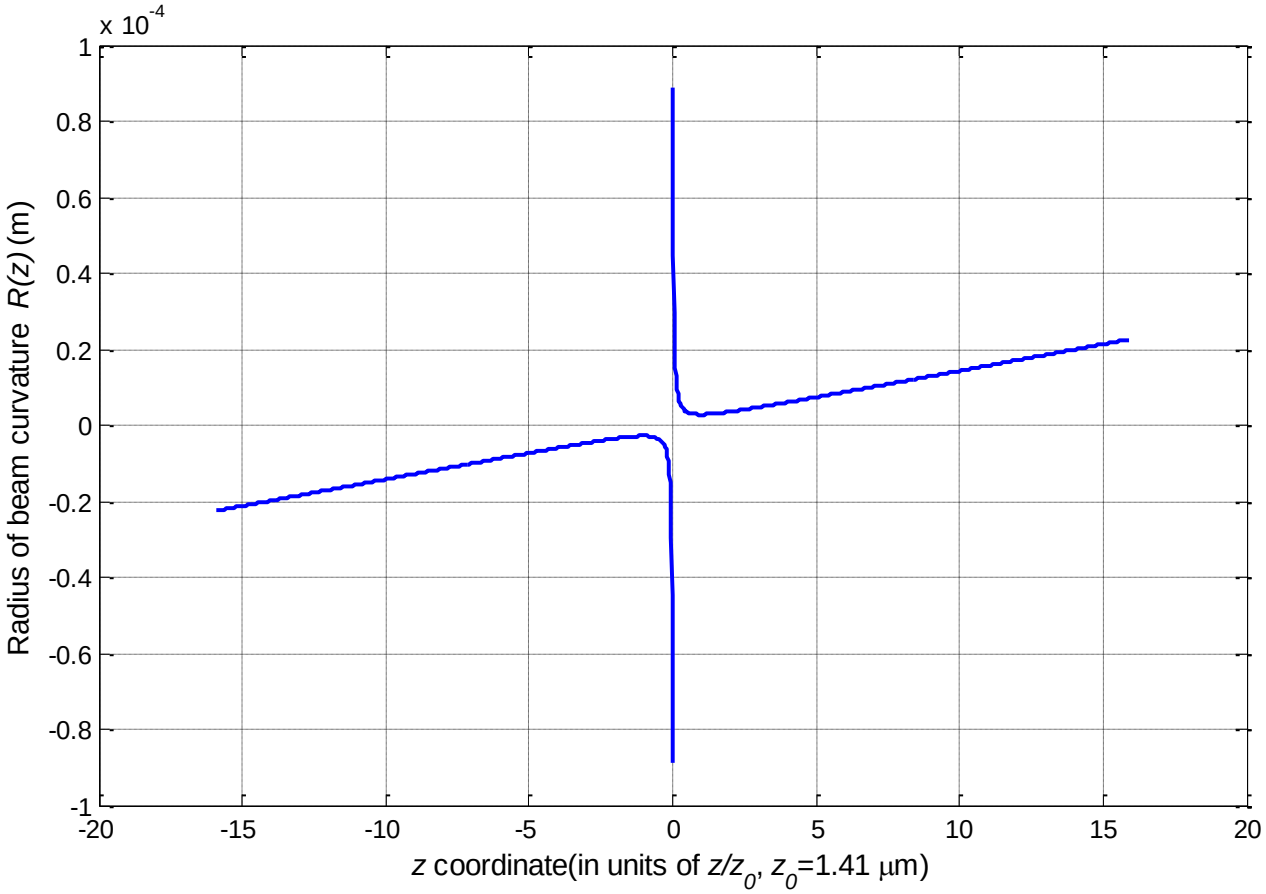

Figure 3. 3 Radius of curvature R(z) of a Gaussian beam.

$$\theta \approx \frac{\lambda}{\pi w_0}, \tag{3.8}$$

where the angle θ is expressed in radians. The beam waist size $w(z)$ grows asymptotically linearly for $z \gg z_0$. Because the divergence is inversely proportional to its minimum waist size, a Gaussian beam that is focused to a small spot size spreads out rapidly as it propagates away from the minimum spot.

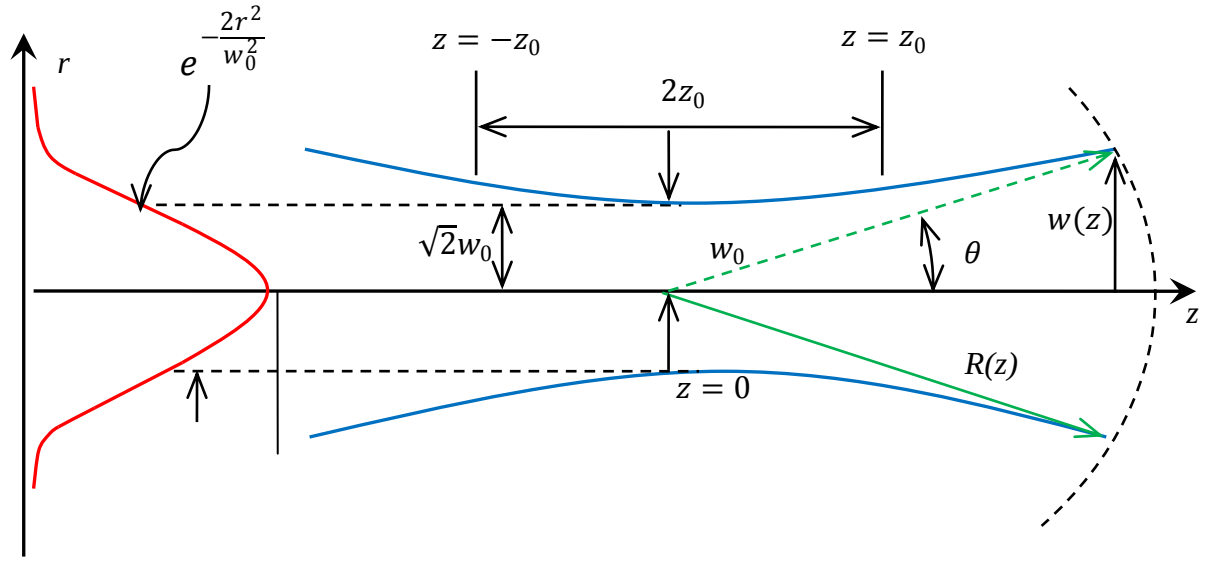

Figure 3. 4 Diagram showing the parameters of the Gaussian beam

3.2.2 Space-time profiles of a space-time Gaussian pulse

Consider a Gaussian pulse given by

$$A(t) = A_0 \exp\left[-\frac{t^2}{2t_0^2}\right] e^{i\omega_0 t}\,, \tag{3.9}$$

where ω_0 is the carrier frequency of the pulse, $1/t_0$ is the $1/e$ bandwidth of the spectrum of the pulse, and A_0 is a constant. The time domain (TD) pulsed field of (3.1) can be derived by the inverse Fourier transform such that :

$$U(r,z,t) = \frac{1}{\sqrt{2\pi}} \int_{-\infty}^{+\infty} U(r,z,\omega) e^{j\omega t}\, d\omega\,. \tag{3.10}$$

To resolve the integral above, Wang *et al.* introduced [43] a complex temporal variable given by

$$\tau(r,z,t) = t - \frac{z + \frac{r^2}{2q(z)}}{c} = t - \frac{z + \frac{r^2}{2R(z)}}{c} + j\frac{r^2}{\omega_0 w^2(z)}\,. \tag{3.11}$$

Then, from (3.1), (3.10) and (3.11) we obtain

$$U(r,z,t) = \frac{w_0}{w(z)} A(\tau) e^{j[\omega_0\tau + \varphi(z)]} \tag{3.12}$$

where, $A(\tau)$ is the inverse Fourier transformation of $A(\omega)$. Then the space-time propagation of the pulse can be obtained by replacing τ with (3.11). By separating the spatial and temporal parts, we get [43]

$$U(r,z,t) = A_0 \frac{w_0}{w(z)} \exp\left[-\frac{\left(t - \frac{r^2}{2cR(z)} - \frac{z}{c}\right)^2}{2t_0^2}\right] \times \exp\left[-\frac{r^2}{w^2(z)} + \frac{r^4}{2w^4(z)}\left(\frac{\delta_0}{\omega_0}\right)^2\right] \times \exp\left\{i\omega_0\left[1 - \frac{r^2}{w^2(z)}\left(\frac{\delta_0}{\omega_0}\right)^2\right]\left[t - \frac{r^2}{2cR(z)} - \frac{z}{c}\right]\right\} \exp[i\varphi(z)]\,, \tag{3.13}$$

where $\delta_0 = 1/t_0$. It is noted from (3.13) that there exists a coupling among the beam parameters in space and time. In other words, the spatial variables r and z emerges in the time shape of the pulse in the first exponential function of (3.13). In addition, a coupling term $\frac{r^2}{w^2(z)}\left(\frac{\delta_0}{\omega_0}\right)^2$, which is related to the bandwidth of the pulse, exists both in the phase and in the spatial distribution of the pulse.

When $z = 0$, the pulsed wave field is not only a function of time but also a function of the radial distance r. Figure 3.5 describes the radial space-time pulse variation, from which it can be seen that the electric field falls off approximately as a Gaussian as r moves away from the axis. A peak frequency of 3.33×10^{14} Hz is used to generate this plot, while the other parameters are $\lambda_0 = 0.449\ \mu$m, w_0=4.05 μm, and the temporal waist size t_0=7.00 fs. When r =22.5μm, which is 5 times the beam waist size w_0, the magnitude of the field is smaller by 13 orders of magnitude compared to the field on the beam axis. Figure 3.6 shows the variation of the field as a function of z at four different times at the $r = 0$ plane.

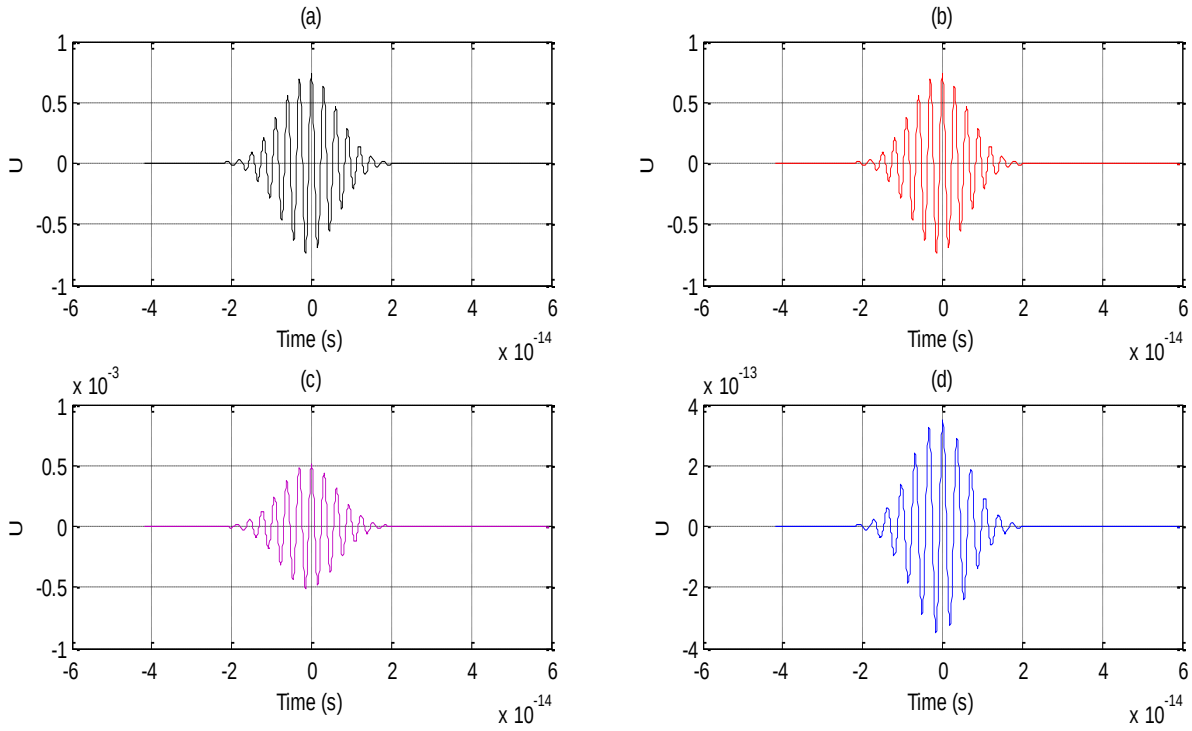

Figure 3. 5 The vertical space-time variation of a Gaussian pulse observed at $z = 0$ and r=0, (b) r =2.25 μm, (c) r =11.25 μm, (d) r =22.5 μm. The spatial and temporal waist sizes are 4.05 μm and 7.00 fs, respectively.

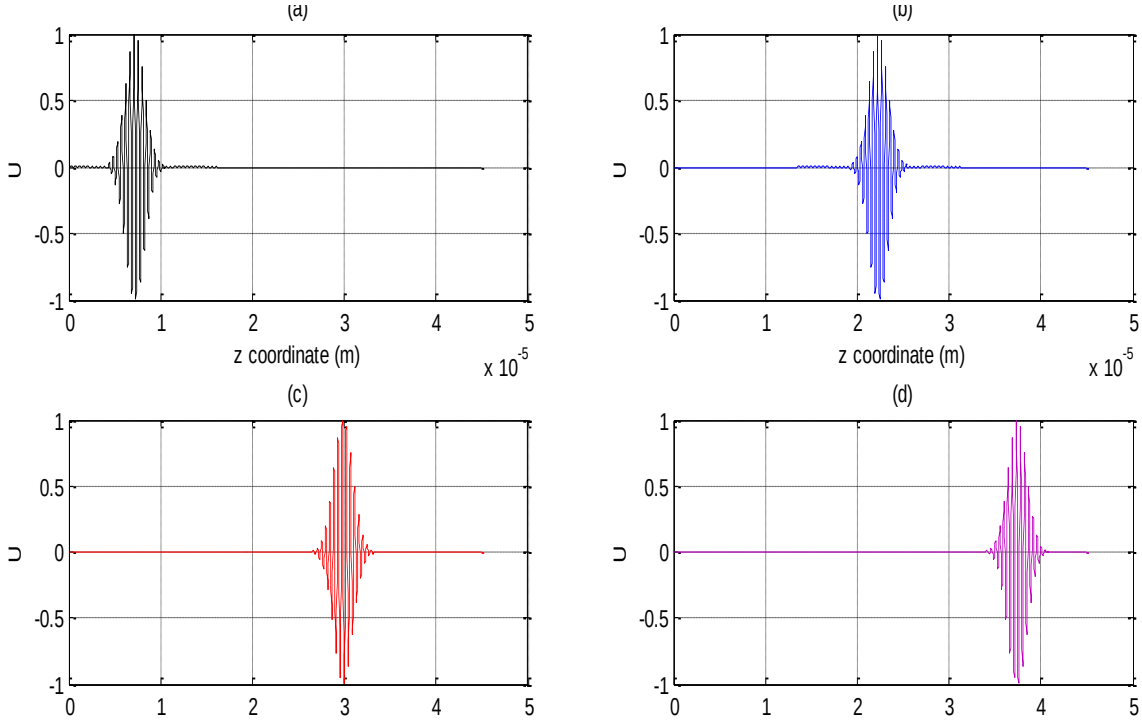

Figure 3. 6 The space-time variation of a Gaussian pulse observed at $r = 0$ and times: (a) $t =$ 0 fs (b) $t = 100$ fs (c) $t = 150$ fs (d) $t = 200$ fs. The spatial and temporal waist sizes are 4.05 μm and 7.00 fs, respectively.

Figure 3.7 shows snapshots from a FDTD simulation of a Gaussian pulsed beam propagating in a homogenous dielectric medium of $\epsilon_r = 4.0$ at various time steps. The x and y axes on the plot corresponds to the propagation distance z and the transverse distance r in the formulation given in (3.13), respectively. The indices shown are spatial indices of the FDTD grid. The grid has been discretized such that there are 20 points per wavelength at the peak frequency of 3.33×10^{14} Hz of the Gaussian beam. The field has been normalized to 0.1 and three decades of logarithmic scaling are used. Thus, on the color bar shown on the right 0 corresponds to a field magnitude of 0.1; -1.0 corresponds to 0.01; -2 corresponds to 0.001; and -3 corresponds to 0.0001. One can see that the field propagation starts from the left most boundary of the rectangular dielectric medium, propagates to the right and is absorbed by the right most boundary using the PML technique discussed in Chap. 2. The beam waist gradually converges to a minimum size at a location corresponds to $z = 0$ and gradually diverges while propagating away from where the minimum waist size occurs.

In the formulation presented by Wang *et al*. the fields begin to diverge when the transverse radial distance r from the beam axis is greater than a certain value. By investigating the governing equation (3.13), from which the FDTD simulation is made, we concluded that this unusual behavior is coming from the term $-\frac{r^2}{w^2(z)} + \frac{r^4}{2w^4(z)}\left(\frac{\delta_0}{\omega_0}\right)^2$ which appears in the second exponential function. One can see that the first part in the term is negative and the power of r is two, while

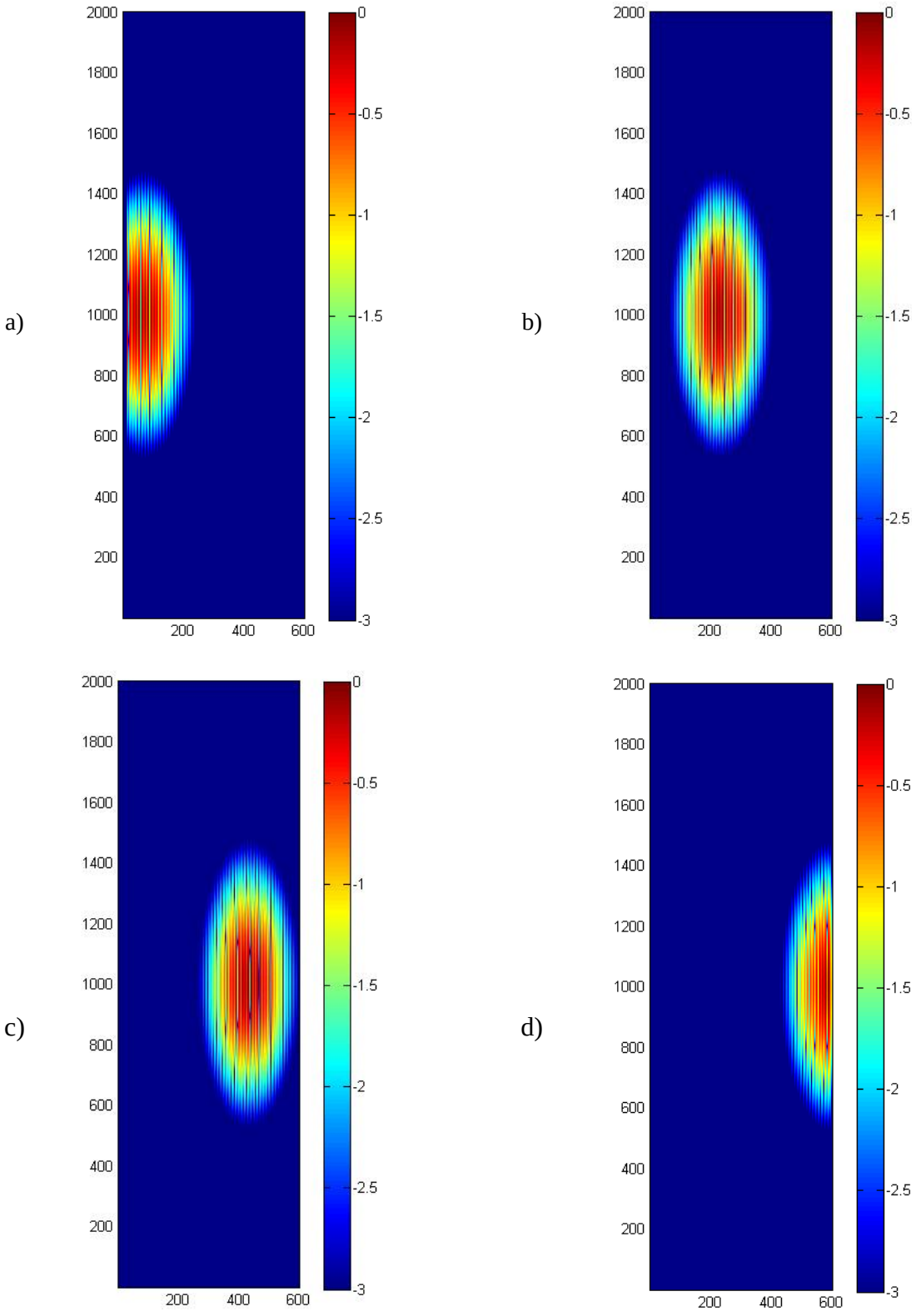

Figure 3. 7 Snapshots from a FDTD simulation of Gaussian pulsed beam propagating in a homogenous dielectric medium.

the second part is positive and the power of r is four. Thus, as r increases from zero, the term decreases to a minimum and then increases without bound.

Let us define a function $f(r)$ such that

$$f(r) = -\frac{r^2}{w^2(z)} + \frac{r^4}{2w^4(z)}\left(\frac{\delta_0}{\omega_0}\right)^2. \tag{3.14}$$

Here, we assumed that, for a given z, $f(r)$ is only a function of the radial distance r from the beam axis. To simplify the problem, we choose $z = 0$ so that $w(z) = w_o$. Thus $f(r)$ becomes:

$$f(r) = -\frac{r^2}{w_0^2} + \frac{r^4}{2w_0^4}\left(\frac{\delta_0}{\omega_0}\right)^2. \tag{3.15}$$

Taking the derivative of $f(r)$ yields:

$$\frac{df}{dr} = -\frac{2r}{w_0^2} + \frac{2r^3}{w_0^4}\left(\frac{\delta_0}{\omega_0}\right)^2. \tag{3.16}$$

Setting $\frac{df}{dr}$=0 and solving for r gives:

$$r = \pm\frac{w_0\omega_0}{\delta_0}. \tag{3.17}$$

Thus, when r increases from zero, $f(r)$ will be negative and gradually decreases to a minimum at $r = \pm\frac{w_0\omega_0}{\delta_0}$, which we label as r_{max}. By plugging in parameters w_0=4.05μm, t_0=7.00 fs (where $\delta_0 = 1/t_0$) and $\omega_0 = 2 \times \pi \times 3.333 \times 10^{14}$ into (3.17), r_{max} is found to be 9.51μm. A plot showing this behavior is shown in Fig. 3.8, in which r_{max} corresponds to the minimum value of $f(r)$. A plot showing the divergence of the field beyond r_{max} is given in Fig. 3.9.

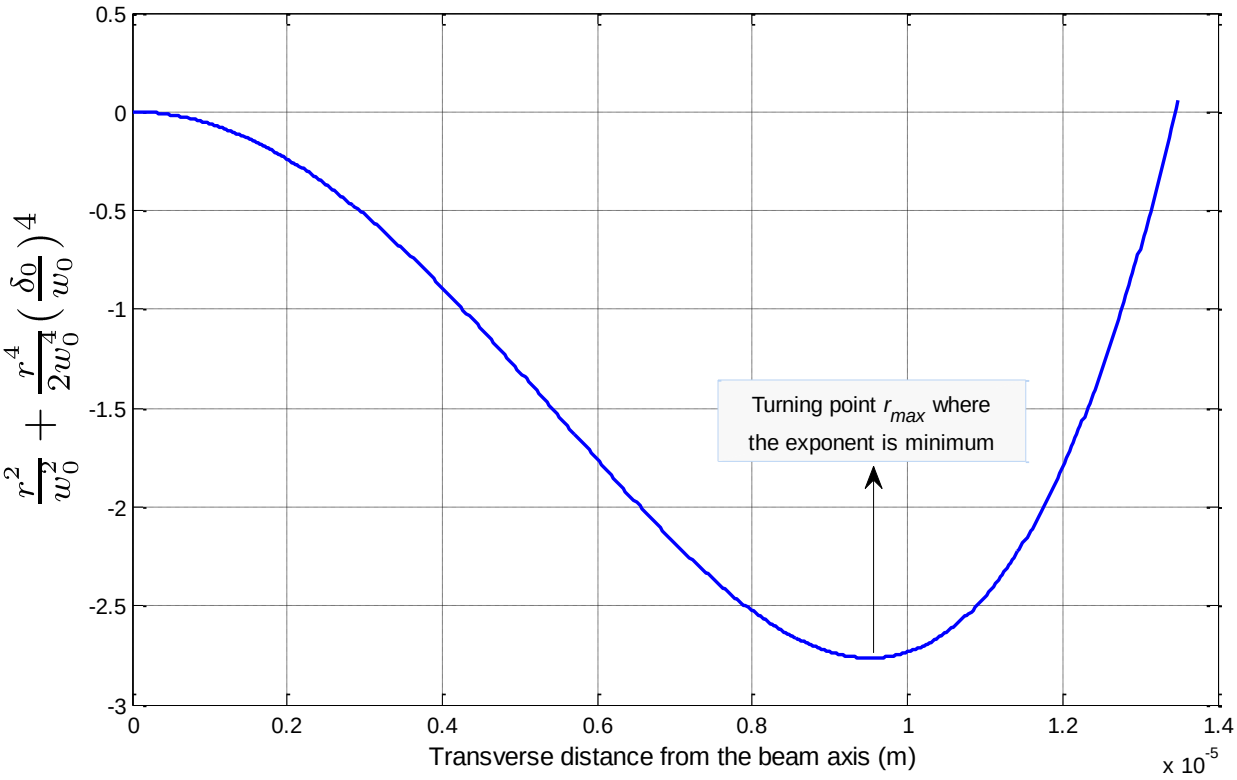

Figure 3. 8 Plot of the exponent of (3.13) that controls the spatial amplitude

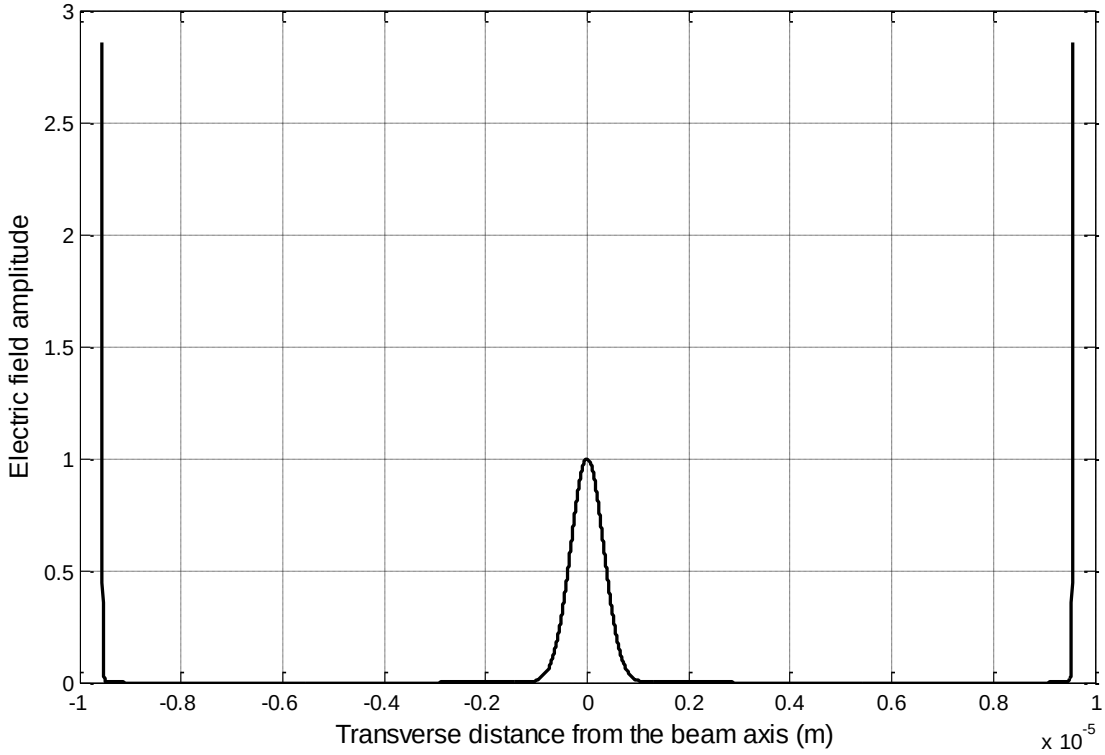

Figure 3. 9 Plot of the field amplitude as a function of transverse distance. The field begins to diverges for $r > r_{max}$.

3.3 Oblique Incidence of the Gaussian Pulsed Beam

In the previous sections we considered a normally incident Gaussian beam. However, in our project, we want a Gaussian beam that can propagate in any direction so that the beam can be obliquely incident upon the interface at an incident angle θ_i relative to the normal to the interface, where $0^\circ < \theta_i < 90^\circ$. In simulations, in order to propagate the wave in an oblique direction, the orientation of the Gaussian beam has to be rotated by angle θ_i relative to the $+z$-axis direction. To simplify the problem, instead of rotating the Gaussian beam orientation, we rotated the coordinate axis by $-\theta_i$ direction where the rotated coordinate axes are given by

$$x = z\cos(-\theta_i) - r\sin(-\theta_i)\,, \tag{3.18}$$

$$y = z\sin(-\theta_i) + r\cos(-\theta_i)\,. \tag{3.19}$$

Here, the original coordinates are in the (z, r) plane and the new coordinates are in the (x, y) plane. Beam parameters are defined in the coordinates whose z axis coincides with the propagation axis of the Gaussian beam. As illustrated in Fig. 3.10, the beam axis and the x axis of the rotated coordinate system form an angle of θ_i. In the FDTD grid, the electric and magnetic field nodes are uniformly spaced.

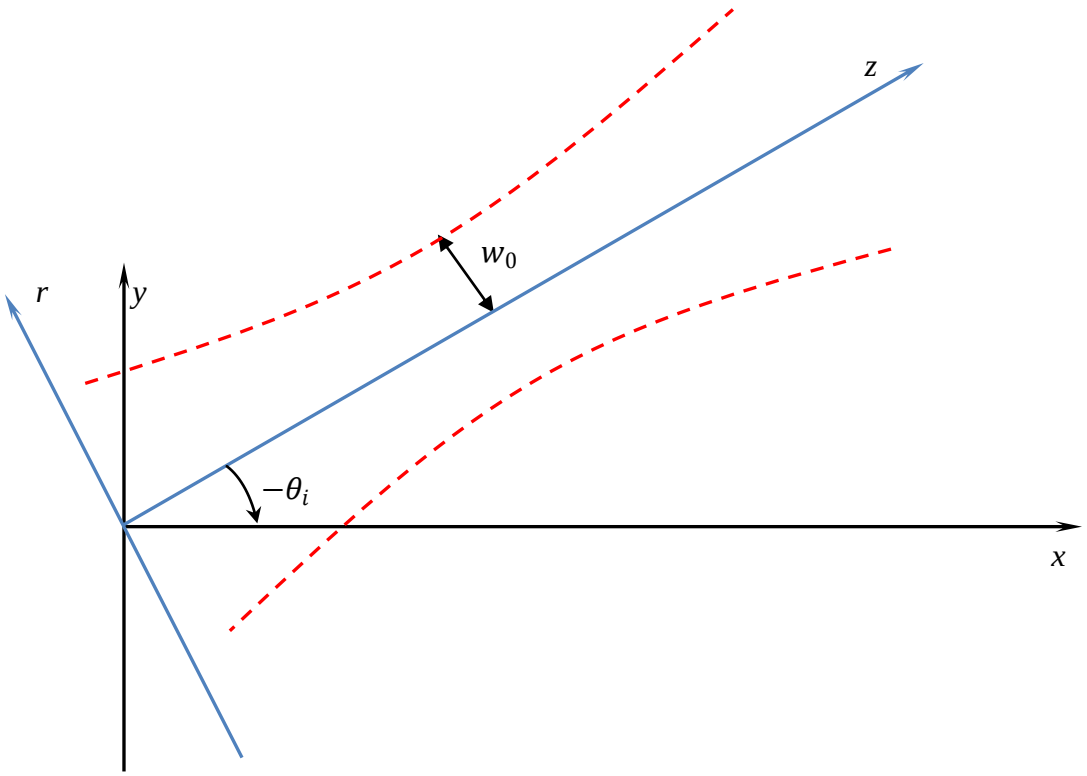

Figure 3. 8 Depiction of the coordinate axis rotation for oblique propagation of a Gaussian beam.

CHAPTER 4
LORENTZIAN MEDIA AND GAINY MATERIALS

4.1 Material Parameters and Conductivity

In the formalization we used so far, we assumed that the material parameters are constant. Such materials are known as simple media. In a simple medium, permittivity ε and permeability μ are scalar constants. If both ϵ and μ are real, and the conductivity is zero, then the medium is lossless. To simplify problems, we often assume that material parameters are constant. However, constant material parameters are an approximation and such materials do not exist in reality. It is impossible to have a lossless dielectric with constant permittivity except for free space. The Kramers-Krönig relations [46][47] shows that the real and imaginary part of the permittivity are related to each other and cannot be independent. For any material other than free space, the loss cannot vanish for all frequencies.

Conductivity is a measure of a material's ability to conduct electric currents. When an electromagnetic wave propagates in a medium, it usually experiences a loss, which is characterized by a positive conductivity $\sigma > 0$. For a material where $\sigma = 0$, electrical energy propagates without loss and the material is called lossless. In some cases, electrical energy will be amplified as it propagates and such materials are called gainy, where the conductivity is $\sigma < 0$. If the material has a non-zero conductivity σ, the current density is given by $\mathbf{J} = \sigma \boldsymbol{E}$. The current density has units of A/m^2 and the conductivity has units of S/m, where the Siemen is defined as 1S=1A/V. In the frequency domain this current density appears in Ampere's law as:

$$\nabla \times \mathbf{H} = \sigma \mathbf{E} + j\omega\epsilon \mathbf{E} = j\omega \left(\epsilon - j\frac{\sigma}{\omega}\right) \mathbf{E} \,. \tag{4.1}$$

Here, the term $\epsilon - j\frac{\sigma}{\omega}$ in parentheses has a real and imaginary part. If we regard it as a single complex number, then it is known as the complex permittivity.

The Faraday's law is :

$$\nabla \times \mathbf{E} = -j\omega\mu\mathbf{H} \,. \tag{4.2}$$

Taking the curl of both sides of (4.2) yields:

$$\nabla \times \nabla \times \mathbf{E} = -j\omega\mu(\nabla \times \mathbf{H}) \,. \tag{4.3}$$

Using a vector identity, the left-hand side of (4.3) can be written as:

$$\nabla \times \nabla \times \mathbf{E} = \nabla(\nabla \cdot \mathbf{E}) - \nabla^2\mathbf{E} \,. \tag{4.4}$$

In a source free region, there are no free charges and hence the term $\nabla \cdot \mathbf{E}$ is zero. Replacing $\nabla \times \mathbf{H}$ in (4.3) with (4.1) yields:

$$-\nabla^2\mathbf{E} = -j\omega\mu\left[(j\omega\left(\epsilon - j\frac{\sigma}{\omega}\right)\mathbf{E})\right], \tag{4.5}$$

and by rearranging the terms, we obtain

$$\nabla^2\mathbf{E} + \omega^2\epsilon\mu\left(1 - j\frac{\sigma}{\omega\epsilon}\right)\mathbf{E} = 0 \,. \tag{4.6}$$

This is the wave equation for **E** in an electrically lossy medium. For propagation only along the x axis, the spatial dependence of **E** is given by $\exp(\pm\gamma x)$ where the propagation constant γ is given by

$$\gamma = j\omega\sqrt{\epsilon\mu\left(1 - j\frac{\sigma}{\omega\epsilon}\right)} = \alpha + jk \,, \tag{4.7}$$

where α (the real part of γ) is the attenuation constant and k (the imaginary part of γ) is the phase constant. When a medium is lossless, the conductivity σ is zero yielding $\gamma = j\omega\sqrt{\epsilon\mu}$, which is equal to j times the phase constant k for a harmonic plane wave.

4.2 Lorentzian Media

The electric flux density for a time-varying electromagnetic field is related to the electric field by

$$\mathbf{D} = \epsilon_0 \mathbf{E} + \mathbf{P}\,, \tag{4.8}$$

where **D** is the electric flux density, **E** is the electric field, and **P** is the polarization vector which accounts for the local displacement of the bound charges in a material. For a dispersive, linear and isotropic material, at a given frequency, the polarization vector is related to the electric field by:

$$\mathbf{P}(\omega) = \chi_e(\omega)\varepsilon_0 \mathbf{E}(\omega)\,, \tag{4.9}$$

where $\chi_e(\omega)$ is the electric susceptibility, which accounts for how easily the charge polarizes in response to an electric field. Putting (4.9) into (4.8) yields:

$$\mathbf{D}(\omega) = \epsilon_0 \mathbf{E}(\omega) + \chi_e(\omega)\varepsilon_0 \mathbf{E}(\omega) = \epsilon_0[1 + \chi_e(\omega)]\mathbf{E}(\omega)\,, \tag{4.10}$$

where the term $1 + \chi_e(\omega)$ is defined as the relative permittivity ϵ_r, so that:

$$\epsilon(\omega) = \epsilon_0 \epsilon_r(\omega) = \epsilon_0[\epsilon_\infty + \chi_e(\omega)]\,, \tag{4.11}$$

where unity is replaced with ϵ_∞ to describe the more general case, which accounts for the effect of the charged material at high frequencies where the susceptibility function goes to zero.

In general, a material cannot polarize instantaneously in response to an applied field. The product of $\chi_e(\omega)$ and $\mathbf{E}(\omega)$ in (4.10) yields a convolution in the time domain. The fields are assumed to be zero prior to $t = 0$, so that

$$\mathbf{D}(t) = \epsilon_0 \mathbf{E}(t) + \varepsilon_0 \int_0^t \chi_e(t')\mathbf{E}(t - t')\, dt'\,, \tag{4.12}$$

where $\chi_e(t)$ is the inverse transform of $\chi_e(\omega)$:

$$\chi_e(t) = \frac{1}{2\pi}\int_{-\infty}^{\infty} \chi_e(\omega) e^{j\omega t}\, d\omega\,. \tag{4.13}$$

In Lorentzian materials, charges are assumed to move under the influence of the electric field but experience a damping (friction) force as well. If the field is oscillating, then any displaced charges will be oscillating also. Therefore, there is a spring force, which wants to bring the charge back to its initial position. Then, the equation of motion for the charges can be expressed as [48]:

$$M\frac{d^2\mathbf{x}}{dt^2} = Q\mathbf{E}(t) - Mg\frac{d\mathbf{x}}{dt} - MK\mathbf{x}\,, \tag{4.14}$$

where M is the mass of the charge, g is the damping coefficient, Q is the amount of charge, and $\mathbf{x}$ is the charge displacement. The last term represents the spring force (which is proportional to the displacement) and is scaled by the spring constant K. The electric susceptibility for Lorentzian materials is given by [48]:

$$\chi_e(\omega) = \frac{\epsilon_l \omega_l^2}{\omega_l^2 + 2jg_l\omega - \omega^2}\,, \tag{4.15}$$

where ω_l is the undamped resonant frequency, g_l is the damping coefficient, and ϵ_l accounts for the relative permittivity at zero frequency. Then, the corresponding relative permittivity is given by:

$$\epsilon_r(\omega) = \epsilon_\infty + \frac{\epsilon_l \omega_l^2}{\omega_l^2 + 2jg_l\omega - \omega^2}\,. \tag{4.16}$$

When the frequency goes to zero, the relative permittivity becomes $\epsilon_\infty + \varepsilon_l$.

4.3 Modeling of Gainy Materials

4.3.1 The auxiliary differential equation method

The FDTD formalism introduced in Chap. 2 is designed for first-order differential equations where the electric or magnetic field is not dependent on extra field components to describe the electromagnetic wave propagation in a medium. However, for electromagnetic waves associated with current density and polarization in a dispersive media, one needs to take special care. The finite difference approximation of the differential equation that relates the polarization and the electric field can be used to obtain polarization at future times in terms of past values and an expression involving the electric field. By doing so, we can obtain a consistent FDTD model in which the electric field and the quantity which relates the electric field to the polarization will be updated simultaneously. This approach is known as the auxiliary differential equation method (ADE). From the mathematics point of view, it stores the first-order derivative of the variable as an extra variable, which reduces the second-order differential equation to two first-order equations. A detailed application of the ADE method to Lorentzian media for a scattered field is discussed in [49].

A gainy material amplifies the power of the incident wave by transferring energy from the material to the propagating wave. Assume a one-dimensional problem with field components E_z and H_y propagating along the x direction through a non-magnetic, isotropic medium. In this case, Maxwell's curl equations are

$$\frac{\partial H_y}{\partial t} = \frac{1}{\mu_0}\frac{\partial E_z}{\partial x}, \tag{4.17}$$

$$J_z + \epsilon_r \epsilon_0 \frac{\partial E_z}{\partial t} = \frac{\partial H_y}{\partial x}. \tag{4.18}$$

The frequency-dependent conductivity that relates the E-field and the current density is given by [50]:

$$\sigma(\omega) = \frac{\mathrm{J}_z(\omega)}{\mathrm{E}_z(\omega)} = \left(\frac{1}{1 + I/I_s}\right)\left[\frac{\sigma_0/2}{1 + j(\omega - \omega_0)T_2} + \frac{\sigma_0/2}{1 + j(\omega + \omega_0)T_2}\right]. \quad (4.19)$$

where Hermitian symmetry is assumed for the Lorentzian gain profile, σ_0 is related to the peak value of the gain set by the pumping level of the excited beam, T_2 accounts for the relaxation process of atoms, ω_0 is the resonant frequency, I_s is the saturation intensity independent of frequency, and I is the spatially dependent intensity. We assumed a saturable, frequency dependent gain through the constitutive relation for the current density. A negative conductance accounts for the gain. Since $\sigma(\omega)$ accounts for any gain (or loss when it is positive) in the medium, the susceptibility will be reduced to a frequency-independent real constant, such that $D_z = \epsilon E_z$, where $\epsilon = \epsilon_r \epsilon_0$.

To investigate how $\sigma(\omega)$ in (4.19) produces gain, separating the right hand side of the equation into real and imaginary parts, we obtain:

$$\begin{aligned}\sigma(\omega) &= \sigma_R(\omega) + j\sigma_I(\omega) \\ &= \frac{\sigma_0[1 + (\omega_0^2 + \omega^2)T_2^2]}{[1 + (\omega_0^2 - \omega^2)T_2^2]^2 + 4\omega^2 T_2^2} + j\,\frac{\sigma_0 \omega T_2[-1 + (\omega_0^2 - \omega^2)T_2^2]}{[1 + (\omega_0^2 - \omega^2)T_2^2]^2 + 4\omega^2 T_2^2}.\end{aligned} \quad (4.20)$$

To be consistent with the previous notation, we assume a propagating wave of the form

$$E_z(x,t) = E_0 e^{-\alpha x} e^{j(\omega t - kx)}, \quad (4.21)$$

where, α is the attenuation constant and k is the phase constant. If the material is low gain such that $\sigma_R(\omega) \ll \omega\epsilon_0\epsilon_{r,\mathrm{eff}}(\omega)$, where

$$\epsilon_{r,\mathrm{eff}}(\omega) = \epsilon_r - j\frac{\sigma_I(\omega)}{\omega\epsilon_0}, \quad (4.22)$$

then α and k are given by

$$\alpha(\omega) \cong \frac{\sigma_R(\omega)}{2c\epsilon_0 n_{\mathrm{eff}}}, \quad (4.23)$$

$$k(\omega) \cong n_{\text{eff}} \frac{\omega}{c}, \tag{4.24}$$

and $n_{\text{eff}} = \sqrt{\epsilon_{r,\text{eff}}}$.

From (4.23) one can see that the attenuation constant $\alpha(\omega)$ will be negative if $\sigma_R(\omega)$ is negative. This results in an increase in the value of $e^{-\alpha x}$ as x increases. This is the case when σ_0 is chosen to be negative.

4.3.2 Analytical simulation of the gain

The behavior of gainy material is illustrated by the plot in Fig. 4.1. A complex-valued propagation constant $\gamma = \alpha + jk$ of a plane wave is computed for a homogenous gainy medium characterized by $\omega_0 = 2\pi \times 3.33 \times 10^{14}$ s^{-1}, $T_2 = 4.7751$ fs, $\epsilon_r = 2.0,$ and $\sigma_0 = -1000$ S/m. The amplification factor $e^{-\alpha l}$ and the phase kl are computed at two points separated by one wavelength in the given medium so that $l = \lambda_0/\sqrt{\epsilon_r}$, where λ_0 is the wavelength in free space that corresponds to ω_0. From Fig. 4.1, one can see that the gain has noticeably increased near the resonant frequency and it has a peak at ω_0.

4.4 Update Equations for Gainy Media

Following the approach given in [50], we will derive a set of update equations for modeling Lorentzian media in the FDTD method. Taking the inverse Fourier transformation of (4.19) yields the following auxiliary differential equation that is solved simultaneously with (4.18):

$$(1 + \omega_0^2 T_2^2) J_z + 2T_2 \frac{\partial J_z}{\partial t} + T_2^2 \frac{\partial^2 J_z}{\partial t^2} = s\sigma_0 E_z + s\sigma_0 T_2 \frac{\partial E_z}{\partial t}. \tag{4.25}$$

where $s = (1 + I/I_s)^{-1}$. In order to write (4.25) in terms of two first-order equations, we define an auxiliary variable F_z:

$$F_z = \frac{\partial J_z}{\partial t}. \tag{4.26}$$

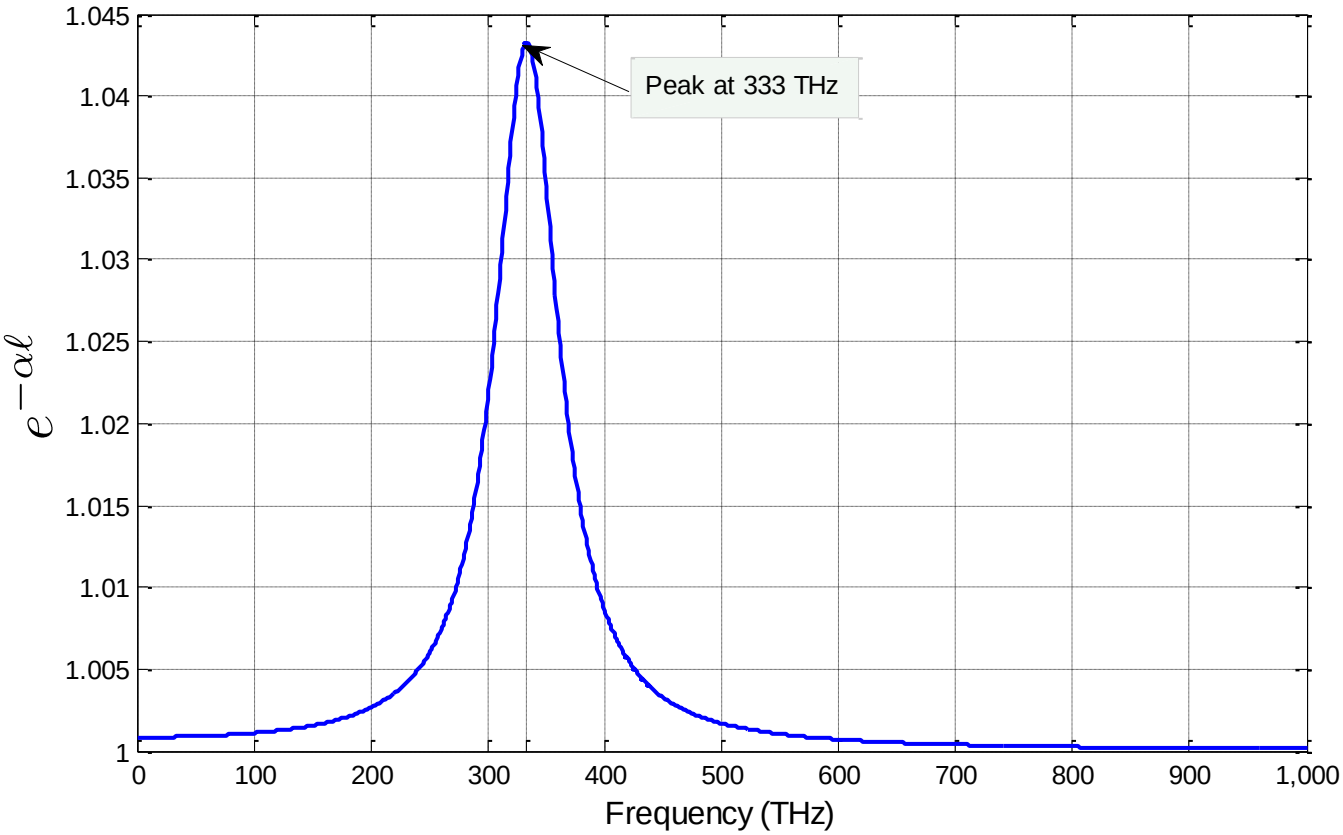

Figure 4. 1 Amplification factor for a distance of one wavelength in a Lorentzian gainy medium where $\sigma_0 = -1000$ S/m.

Then by plugging F_z into (4.25):

$$(1 + \omega_0^2 T_2^2) J_z + 2T_2 F_z + T_2^2 \frac{\partial F_z}{\partial t} = s\sigma_0 E_z + s\sigma_0 T_2 \frac{\partial E_z}{\partial t}. \tag{4.27}$$

The coupled differential equations (4.18), (4.26) and (4.27) can be converted to finite difference expressions using second-order central differences at time step $q + 1/2$. Since the approach to derive finite difference expressions are discussed in detail in Chap. 2, we will not list all the steps of deriving the update equations here. Because the temporal derivative of the electric field is given by

$$\frac{\partial E_z}{\partial t} = \frac{1}{\epsilon} \frac{\partial H_y}{\partial x}, \tag{4.28}$$

the $\frac{\partial E_z}{\partial t}$ term in (4.27) can be replaced by $\frac{1}{\epsilon} \frac{\partial H_y}{\partial x}$. Solving for $\frac{\partial F_z}{\partial t}$ in (4.27) yields

$$\frac{\partial F_z}{\partial t} = \left(s\sigma_0 T_2 \frac{1}{\epsilon} \frac{\partial H_y}{\partial x} + s\sigma_0 E_z - (1 + \omega_0^2 T_2^2) J_z - 2T_2 F_z \right) T_2^{-2} . \tag{4.29}$$

Expressing the derivatives in terms of finite differences:

$$\frac{\partial F_z}{\partial t} = \frac{F_z|_m^{q+1} - F_z|_m^q}{\Delta t}, \qquad \frac{\partial H_y}{\partial x} = \frac{H_y|_{m+1/2}^{q+1/2} - H_y|_{m-1/2}^{q+1/2}}{\Delta x}, \tag{4.30}$$

where Δx is the spatial offset between sample points and Δt is the temporal offset. The index m corresponds to the spatial step in the x direction, while the index q corresponds to the temporal step. After replacing the derivatives in (4.29) with (4.30) one can obtain the update equation for F_z. The update equation for J_z can be derived from (4.27) by replacing the derivative $\frac{\partial J_z}{\partial t}$ with $\frac{J_z|_{m,n}^{q+1} - J_z|_{m,n}^q}{\Delta t}$. The update equation for E_z has the standard form discussed in Chap. 2, with an extra current term.

Note that the formalism we have developed in this chapter is for one-dimensional problems where propagation is along the x direction and the only components are E_z and H_y. However, in our project, we want to use a two-dimensional TMz grid where the non-zero fields are E_z, H_y and H_x. By incorporating the H_x field into the expressions for $F_z|_{m,n}^{q+1}$, $J_z|_{m,n}^{q+1}$ and $E_z|_{m,n}^{q+1}$ we obtain the following equations:

$$\begin{aligned} F_z|_{m,n}^{q+1} = {} & A_1 \left[\left(H_y|_{m+1/2,n}^{q+1/2} - H_y|_{m-1/2,n}^{q+1/2} \right) - \left(H_x|_{m,n+1/2}^{q+1/2} - H_x|_{m,n-1/2}^{q+1/2} \right) \right] \\ & + A_2 E_z|_{m,n}^q + A_3 J_z|_{m,n}^q + A_4 F_z|_{m,n}^q , \end{aligned} \tag{4.31}$$

$$J_z|_{m,n}^{q+1} = J_z|_{m,n}^q + \frac{\Delta t}{2} \left(F_z|_{m,n}^{q+1} + F_z|_{m,n}^q \right), \tag{4.32}$$

$$\begin{aligned} E_z|_{m,n}^{q+1} = {} & E_z|_{m,n}^q \\ & + \frac{\Delta t}{\epsilon \Delta x} \left[\left(H_y|_{m+1/2,n}^{q+1/2} - H_y|_{m-1/2,n}^{q+1/2} \right) - \left(H_x|_{m,n+1/2}^{q+1/2} - H_x|_{m,n-1/2}^{q+1/2} \right) \right] \end{aligned} \tag{4.33}$$

$$-\frac{\Delta t}{2\epsilon}\left(J_z|_{m,n}^{q+1}+J_z|_{m,n}^{q}\right),$$

$$A_1=\frac{4\Delta t s(m,n)\sigma_0(\Delta t+2T_2)}{B\Delta x}, \tag{4.34}$$

$$A_2=\frac{8\epsilon s(m,n)\sigma_0\Delta t}{B}, \tag{4.35}$$

$$A_3=-\frac{4\Delta t[2\epsilon(1+\omega_0^2T_2^2)+s(m,n)\sigma_0(\Delta t+2T_2)]}{B}, \tag{4.36}$$

$$A_4=-\frac{8\epsilon T_2(\Delta t-T_2)+(\Delta t)^2[2\epsilon(1+\omega_0^2T_2^2)+s(m,n)\sigma_0(\Delta t+2T_2)]}{B}, \tag{4.37}$$

$$B=8\epsilon T_2(\Delta t+T_2)+(\Delta t)^2[2\epsilon(1+\omega_0^2T_2^2)+s(m,n)\sigma_0(\Delta t+2T_2)], \tag{4.38}$$

$$s(m,n)=[1+I(m,n)/I_s]^{-1}, \tag{4.39}$$

$$I(m,n)=0.5cn\epsilon_0(E_z|_{m,n}^{peak})^2. \tag{4.40}$$

Here, the saturation constant $s(m,n)=1$ for linear medium, since the intensity is negligible compared to the saturation intensity. In a linear medium, a material's permittivity and/or permeability varies with frequency at low intensities of the wave's E- and/or H-fields [50].

The update equations for the magnetic field component H_x and H_y are given at time-step $q+\frac{1}{2}$ in the standard approach discussed in Chap. 2, where the magnetic field parameters are assumed to be constant:

$$H_x|_{m,n+1/2}^{q+1/2}=H_x|_{m,n+1/2}^{q-1/2}+\frac{\Delta t}{\mu_0\Delta x}\left(E_z|_{m,n+1}^{q}-E_z|_{m,n}^{q}\right), \tag{4.41}$$

$$H_y|_{m+1/2,n}^{q+1/2}=H_y|_{m+1/2,n}^{q-1/2}+\frac{\Delta t}{\mu_0\Delta x}\left(E_z|_{m+1,n}^{q}-E_z|_{m,n}^{q}\right). \tag{4.42}$$

We see that the algorithm to model a Lorentzian media in the FDTD method is a five-step process given by (4.31), (4.32), (4.33), (4.41) and (4.42).

CHAPTER 5
FDTD ANALYSIS OF GAUSSIAN BEAM REFLECTION

5.1 Evanescent Field

As discussed in Chap. 1, total internal reflection (TIR) occurs when light hits a boundary between materials of higher and lower refractive indices when the incident angle is greater than the critical angle. An important side effect of TIR is the existence of an evanescent field across the boundary. Essentially, even though the entire incident wave is reflected back into the originating medium, there is some penetration into the second medium. The chief distinction of the evanescent field is that its amplitude decays exponentially and, assuming lossless media, the field itself does not propagate.

Let us consider two dielectric media with refractive indices n_1 and n_2 respectively, as shown in Fig. 5.1. A plane wave strikes the boundary between the two media at the incident angle θ_i with respect to the normal where the interface is along the y axis and the normal is along the x axis. The angle of the reflected plane wave θ_r is equal to θ_i. The angle of the transmitted field is related to θ_i by Snell's law so that $\sin\theta_t = \frac{n_1}{n_2}\sin\theta_i$ and

$$\cos\theta_t = \sqrt{1-\sin^2\theta_t} = \sqrt{1-\left(\frac{n_1}{n_2}\sin\theta_i\right)^2}. \tag{5.1}$$

When θ_i is greater than the critical angle θ_c (which is equal to $\sin^{-1}\left(\frac{n_2}{n_1}\right)$) then $\cos\theta_t$ will be imaginary so that

$$\cos\theta_t = j\sqrt{\left(\frac{n_1}{n_2}\sin\theta_i\right)^2-1}\,. \tag{5.2}$$

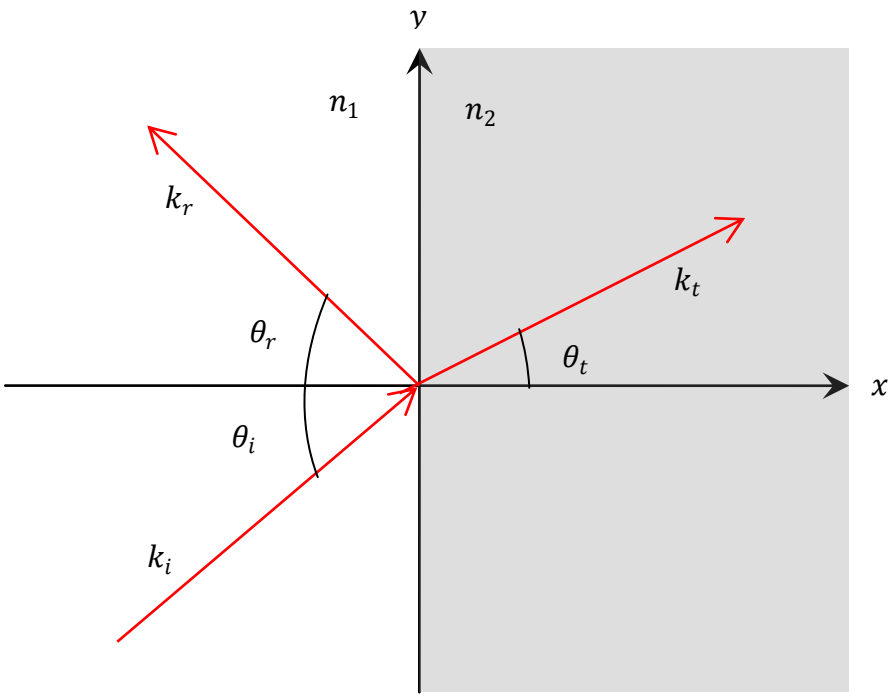

Figure 5. 1 A plane wave at the boundary of two dielectric media.

Assuming $\exp(j\omega t)$ for the temporal dependence, the spatial dependence for the incident, reflected, and transmitted fields are given by $\exp(-j\mathbf{k}_i \cdot \mathbf{r})$, $\exp(-j\mathbf{k}_r \cdot \mathbf{r})$, and $\exp(-j\mathbf{k}_t \cdot \mathbf{r})$ respectively, where $\mathbf{k}_i = (k_{ix}, k_{iy})$, $\mathbf{k}_t = \left(k_{tx}, k_{ty}\right) = (k_t \cos\theta_t, k_t \sin\theta_t)$, and $\mathbf{r} = (x, y)$. The reflected field wave vector differs from the incident wave vector only in the sign of the x components and $|k_i| = |k_r| = \frac{\omega}{c} n_1$, $|k_t| = \frac{\omega}{c} n_2$.

Now we can write the transmitted wave (s –polarized) as

$$E_t = E_{0t} e^{j(\mathbf{k}_t \cdot \mathbf{r} - \omega t)}, \tag{5.3}$$

$$= E_{0t} e^{j k_t \cos\theta_t x + j k_t \sin\theta_t y - j\omega t}, \tag{5.4}$$

$$= E_{0t} e^{j k_t \cos\theta_t x} e^{j k_t \sin\theta_t y} e^{-j\omega t}, \tag{5.5}$$

$$= E_{0t} e^{-k_t x \sqrt{\left(\frac{n_1}{n_2}\sin\theta_i\right)^2 - 1}} e^{j k_t \sin\theta_t y} e^{-j\omega t}, \tag{5.6}$$

$$= E_{0t} e^{-k_t x \sqrt{\left(\frac{n_1}{n_2}\sin\theta_i\right)^2 - 1}} e^{j(k_{ty} y - \omega t)}. \tag{5.7}$$

From (5.7) one can note that the effect of the term $e^{-k_t x \sqrt{\left(\frac{n_1}{n_2}\sin\theta_i\right)^2 - 1}}$ is an exponential decay. As x increases, the amplitude of the field decays exponentially. Therefore, there is a transmitted field in TIR with a exponential decay in amplitude, which is referred to as the evanescent field. Figure 5.2 shows the exponential decay of the evanescent wave intensity from an interface of two dielectrics where $n_1 = 4$, $n_2 = 2$ and the frequency is 3.33×10^{14} Hz. The field is introduced at an incident angle of 46°, where the critical angle is 45°.

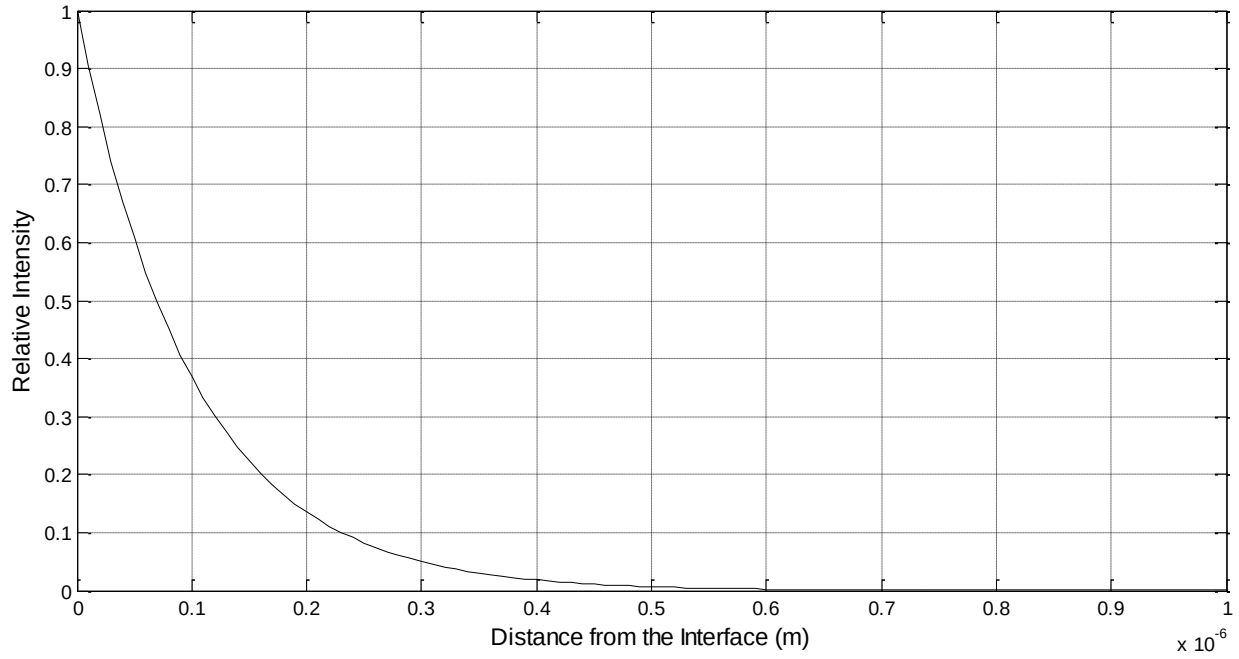

Figure 5. 2 Exponential decay of evanescent field.

5.2 FDFD Simulation of Gaussian Beam Reflection

5.2.1 System under consideration

In this project, we used a Gaussian beam to determine the reflection coefficient associated with a gainy medium. We considered a region composed of two dielectric half spaces, where the two half spaces have an interface at $x = 0$. Medium 1 and medium 2 are located to the left and to the right of the interface, respectively, as shown in Fig. 5.3. To get information purely concerning reflection from the interface from the two media, medium 2 is extended to infinity along the x direction, so that we can avoid the contribution of reflection from the edge of the medium 2. Both media are non-magnetic. Medium 1 has dielectric constant ε_{r1} and conductivity σ_1, where we set $\sigma_1 = 0$ so that it is lossless. Medium 2 is assumed to be a single-pole Lorentzian material

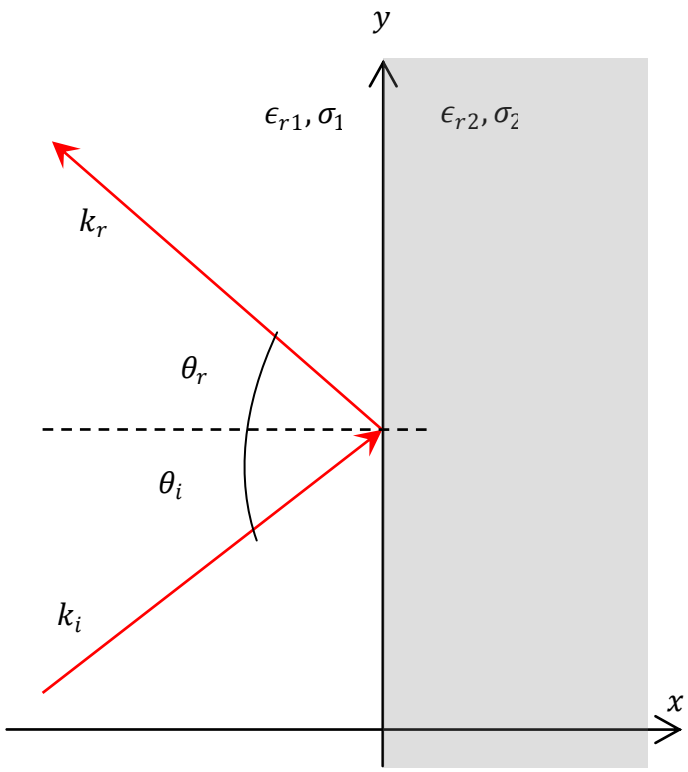

Figure 5. 3 System under consideration.

where the permittivity ϵ_2 and the conductivity σ_2 are dependent on frequency. However, we require the effective permittivity $\epsilon_{r,\text{eff}}$, specified in (4.22), of medium 2 to be smaller than ε_{r1} so that TIR can occur. Medium 2 is either lossy if $\sigma_2 > 0$ or gainy if $\sigma_2 < 0$. Willis *et al.* has reported results [15] from a similar system, but in their consideration, the conductivity σ_2 is taken to be a constant independent of frequency. We made simulations first following Willis' approach and obtained identical results to theirs. Finally, the results from the constant and Lorentzian media are compared.

5.2.2 FDTD grid and parameters set up

To investigate the reflection coefficient from a Lorentzian gainy (or lossy) medium, we used a 2D TMz FDTD grid with non-zero field components of E_z, H_x and H_y. Both half spaces are non-magnetic. Medium 1 is set to be lossless and has a dielectric coefficient $\varepsilon_{r1} = 4$. The discretization is set to 20 points per wavelength for a pulsed Gaussian beam with a Gaussian envelope and carrier frequency of $f_0 = 3.333 \times 10^{14}$ Hz. The spatial waist size is 9 wavelengths. The Courant number is $0.95/\sqrt{2}$ in free space so that the spatial and temporal resolution of the FDTD gird is calculated to be $\Delta x = \Delta \text{y} = 22.487$ nm and $\Delta t = 5.0386 \times 10^{-17}$s.

Medium 2 is assumed to be filled with a homogenous gainy (or lossy) medium characterized by $\lambda_0 = 636$ nm, $T_2 = 4.7751$ fs, $\epsilon_r = 2.0$ and $\sigma_0 = \pm 1000$ S/m, where the upper sign of σ_0 is taken for lossy medium and the lower sign is taken for gainy medium. For a description of these parameters, see Sec. 4.3.1. With these parameters, at a frequency of 3.333×10^{14} Hz, the medium has an effective permittivity $\epsilon_{r,\text{eff}}$ of 2.0, a conductivity σ_2 of -500 S/m (for $\sigma_0 = -1000$) or 500 S/m (for $\sigma_0 = 1000$). The critical angle is 45°.

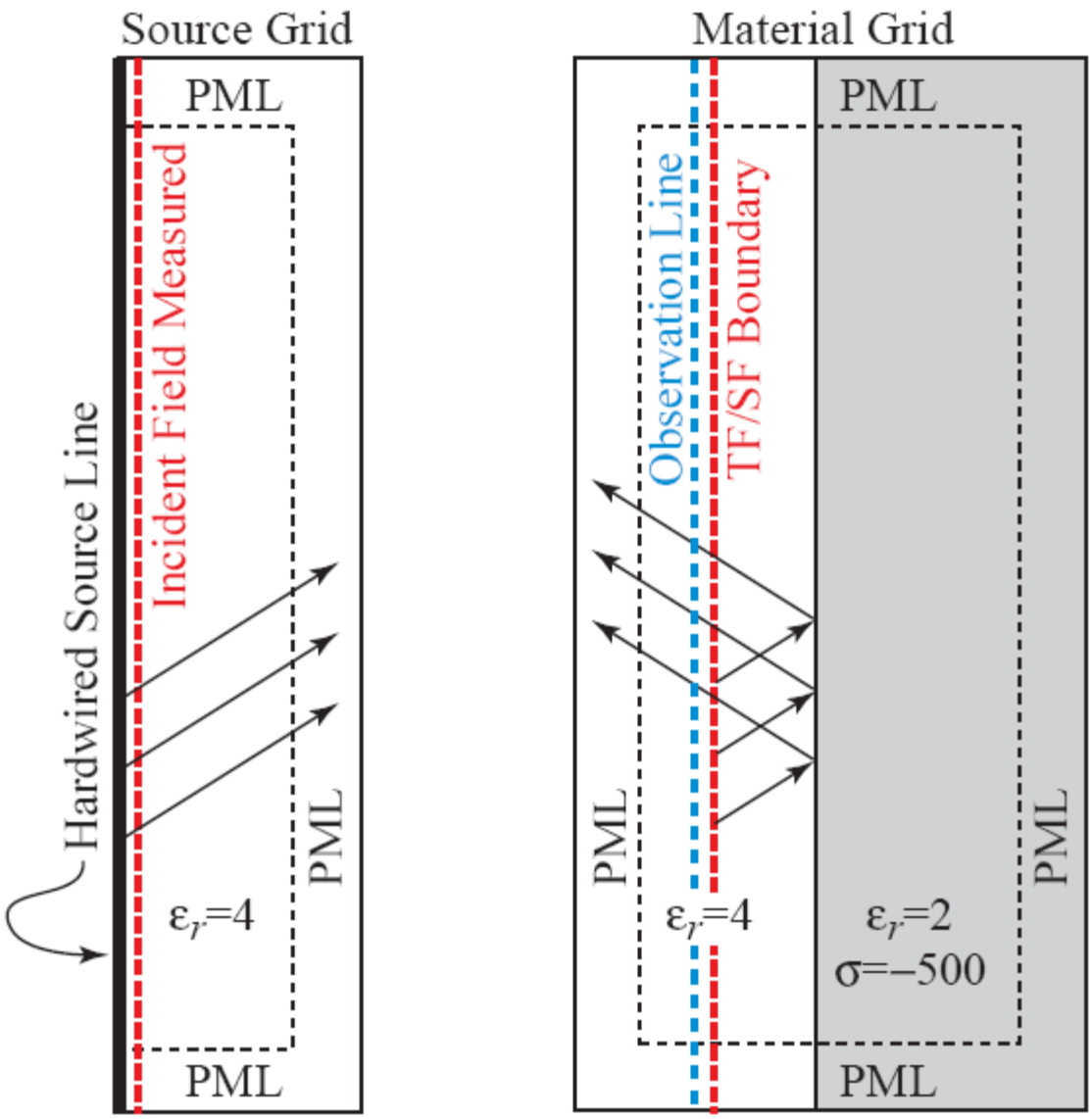

Figure 5. 4 FDTD grid set up.

The diagrams of Fig. 5.4 describe the configuration of the FDTD grids used in the simulations. There are two grids to model the interaction process. The grid to the left is an auxiliary source grid that is used to model the incident field, and the grid to the right is the main material grid that is used to model the interaction. The purpose of using the source grid is solely to calculate the incident field. All boundaries of both grids (except for the left edge of the source

grid) are terminated with perfectly matched layers (PML) absorbing boundary conditions which are designed to absorb out-ward propagating fields. The PML absorbing boundary technique is a state-of-the-art technique which was discussed in Chap. 2. In the source grid, the source is hard-wired to the left boundary so that the Gaussian beam is emitted from the left, propagates to the right, and gets absorbed by the PML boundary. This grid is very narrow, with a computational domain of 31×2001 cells. The direction of propagation will be determinded by defining an incident angle so that it can be propagated in any direction.

The Gaussian beam is introduced to the material grid via a total-field/scattered-field (TF/SF) boundary which separates the material grid into a total-field (TF) and a scattered-field (SF) region, where the TF region contains both the incident and scattered field and the SF region only contains the scattered field. The TF/SF boundary is set a few cells away from the interface between the lossless and Lorentzian half spaces, so that the incident field interacts with the interface just after being introduced to the material grid. The computational domain of the material grid is 151×2001 cells, where the TF/SF boundary is located 12 cells away from the left boundary. The interface between the two media is located 2 cells to the right of the TFSF boundary and the observational line to measure the scattered field is located 2 cells to the left of the TFSF boundary. Therefore, in the material grid, the field is introduced via the TF/SF boundary, propagates to the right, reflects back from the interface and gets absorbed by the PML boundaries. In the case of evanescent decay, more than 7 wavelengths at the peak frequency of the pulse in medium 2 are between the interface and the right-hand PML boundary so that the majority of the decaying field will be represented within the FDTD grid. Figures 5.5 to 5.7 show snapshots of the Gaussian beam propagation obtained from simulations at different time-steps,

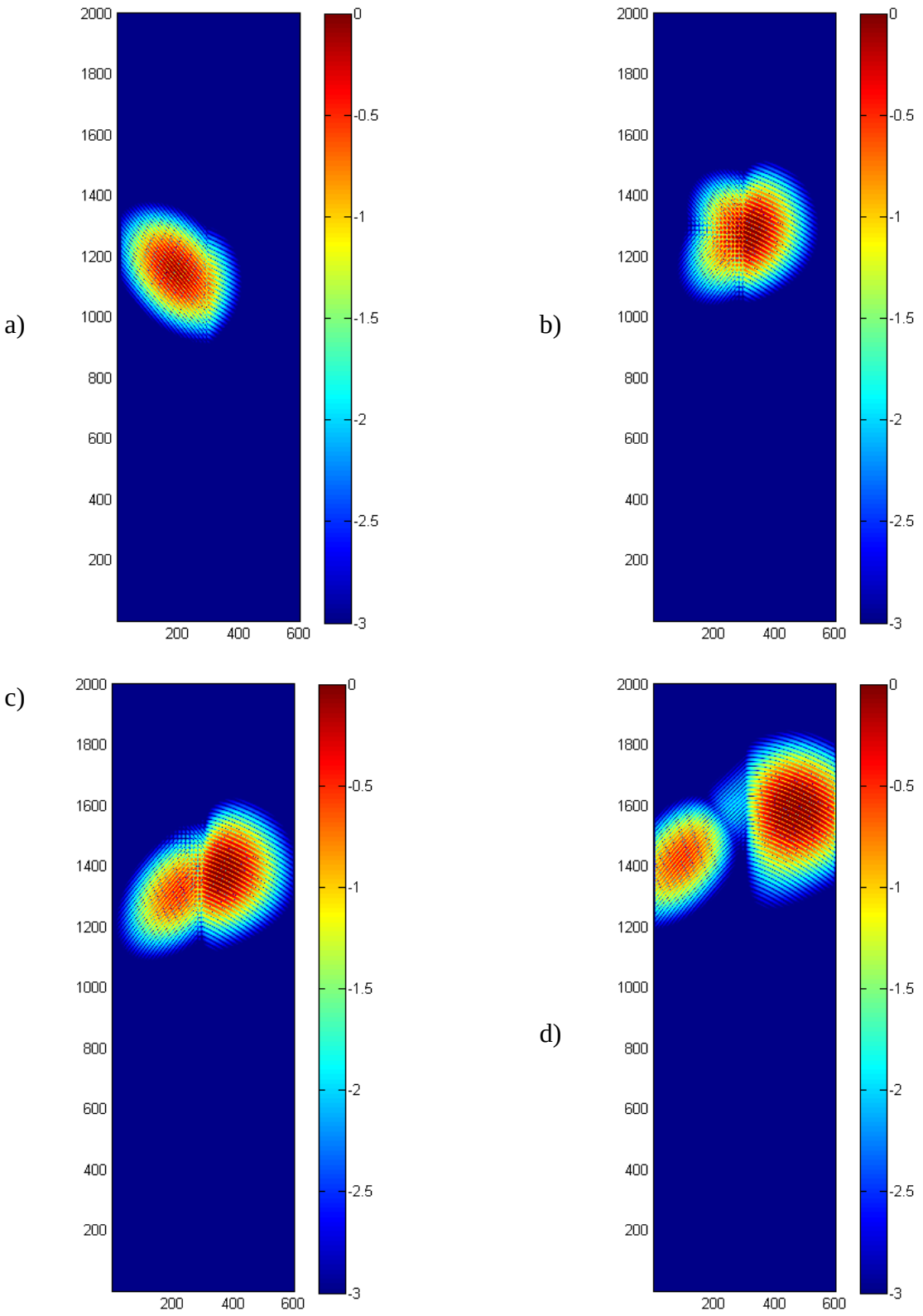

Figure 5. 5 Snapshots of the electric field at time-steps a) 2500 b) 3000 c) 3250 d) 3750. The incident angle is 40 degrees. The material is gainy.

a)

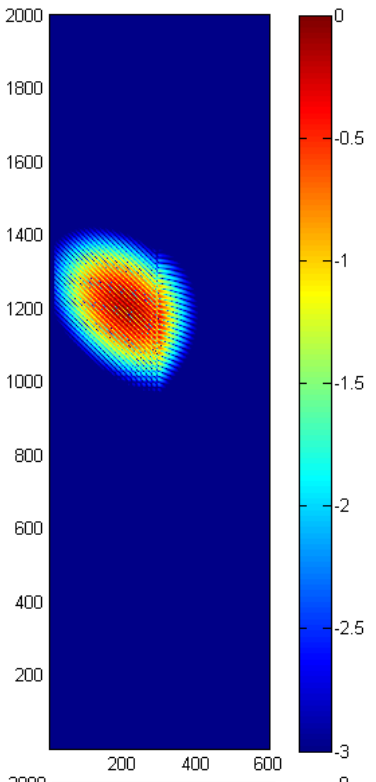

b)

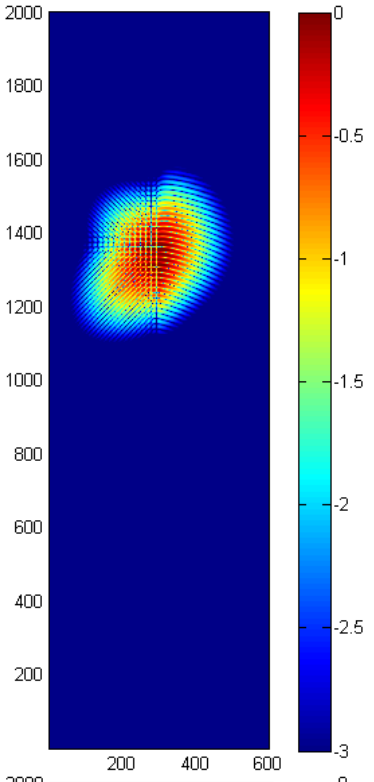

c)

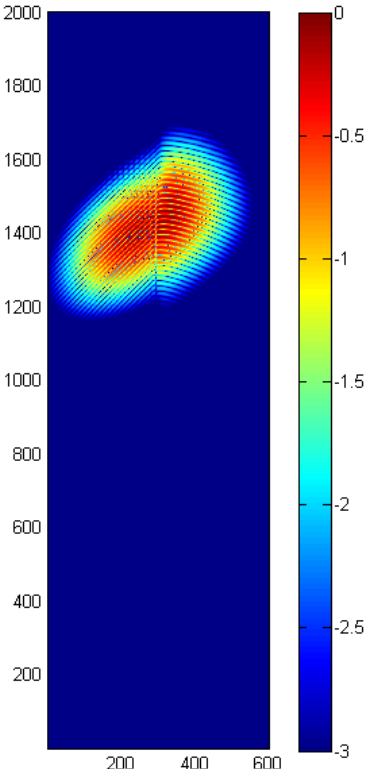

d)

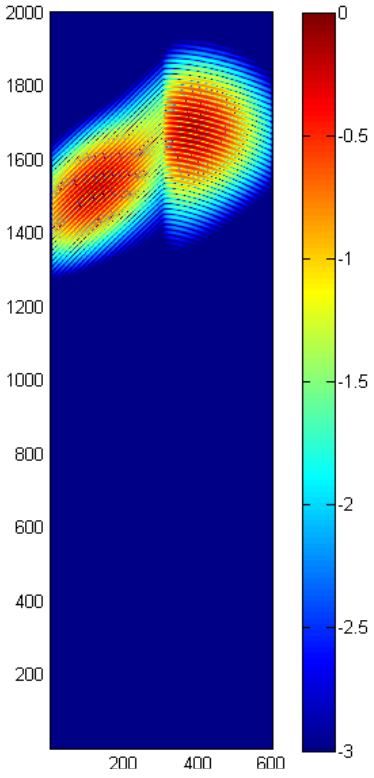

Figure 5. 6 Snapshots of the electric field at time-steps a) 2700 b) 3200 c) 3500 d) 4000. The incident angle is 46 degrees. The material is gainy.

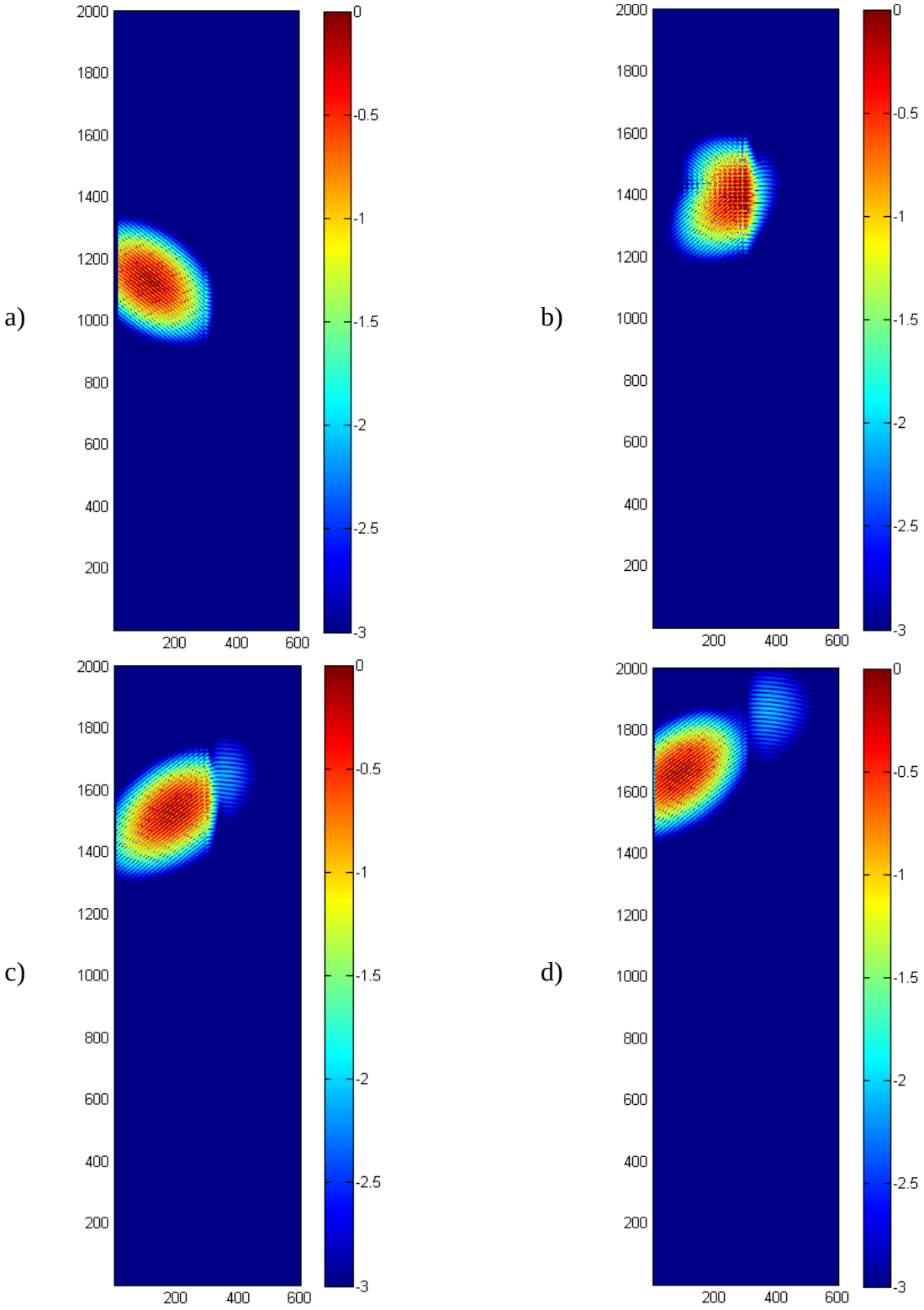

Figure 5. 7 Snapshots of the electric field at time-steps a) 2500 b) 3500 c) 4000 d) 4500. The incident angle is 52 degrees. The material is gainy.

for incident angles of 40, 56, and 52 degrees, respectively. The field has been normalized to 0.1 and three decades of logarithmic scaling are used. Thus, on the color bar shown on the right 0 corresponds to a field magnitude of 0.1; -1 corresponds to 0.01; -2 corresponds to 0.001; and -3 corresponds to 0.0001. In Fig. 5.6 and Fig. 5.7, the field to the right of the interface is primarily an evanescent wave that decays exponentially. One can see that the amount of decay for 52 degrees is much more than for 46 degrees. The field to the right of the interface in the 40 degrees case is the transmitted wave propagating in the second medium.

5.2.3 Reflection coefficient calculation

In the source grid, the incident field is measured right after the Gaussian beam is emitted, where the observation line is one cell away from the source line, as shown in Fig. 5.4. In the material grid, the reflected field is measured at the observation line that is located 2 cells to the left of the TF/SF boundary, as shown in Fig. 5.4. The observation lines run through the centers of the Yee grid cells so that the E_z components are located on the observation lines and the H_x components are positioned a spatial half-step to either side of the line. A discrete Fourier transformation (DFT) is used to obtain the spectral information at the carrier frequency f_0 from the time-domain data, where a running DFT is incorporated in the FDTD code so that the Fourier transformation is performed during the time-stepping loop. Because the magnetic field is not aligned with the observation line, the geometric mean is taken of the magnetic fields to either side of the line, which has been shown to be more accurate than taking an arithmetic mean [51]. The FDTD method intrinsically implies that the electric field and the magnetic fields cannot be recorded at the same time step, e.g., assume the electric fields have been recorded at times of $q = 1,2,3, \ldots$, then the magnetic field will be recorded at times of $q = \frac{1}{2}, \frac{3}{2}, \frac{5}{2}, \ldots$. To account for this temporal offset, after obtaining the spectral representation of the electric and magnetic field, the phasors of

E_z are multiplied by a phase factor so that all field components use a common temporal reference point.

These collocated fields are used to calculate the x-directed power density at each point along the observation line using the Poynting vector $\frac{1}{2}\mathrm{Re}(\mathbf{E} \times \mathbf{H}^*)$[52]. The power density values at each point along the observation lines are integrated to compute the x-directed power that passes across each line, where the integration along the observation lines in the source grid and the material grid gives the incident and reflected power, respectively. The square root of the ratio of the reflected power to the incident power yields the magnitude of the reflection coefficient.

5.3 Theoretical Analysis of Gaussian Beam Reflection

As stated in Chap. 1, the sign choice of the conductivity in the conventional Fresnel equation does not affect the magnitude of the reflection coefficient. Nevertheless, as can be seen from Willis *et al.*'s result [15], the sign choice has a critical effect on the reflection coefficient. The detailed mathematical justification for the sign choice is discussed in [15], where a new branch cut for the valid range of the argument of the complex wave number in the second medium is defined. We follow that approach to get a theoretical result for plane wave reflection from an interface.

The incident pulsed Gaussian wave can be represented as a continuous spectrum of plane waves as shown in Fig 5.8 [15], where the x and y axes are normal and tangential to the interface, respectively. The X and Y axes are for oblique incidence, where the coordinate axes are rotated, as discussed in Chap. 3. The central beam axis is aligned with the X axis forming the angle θ_i between the x and X axis. The incident field can be written as

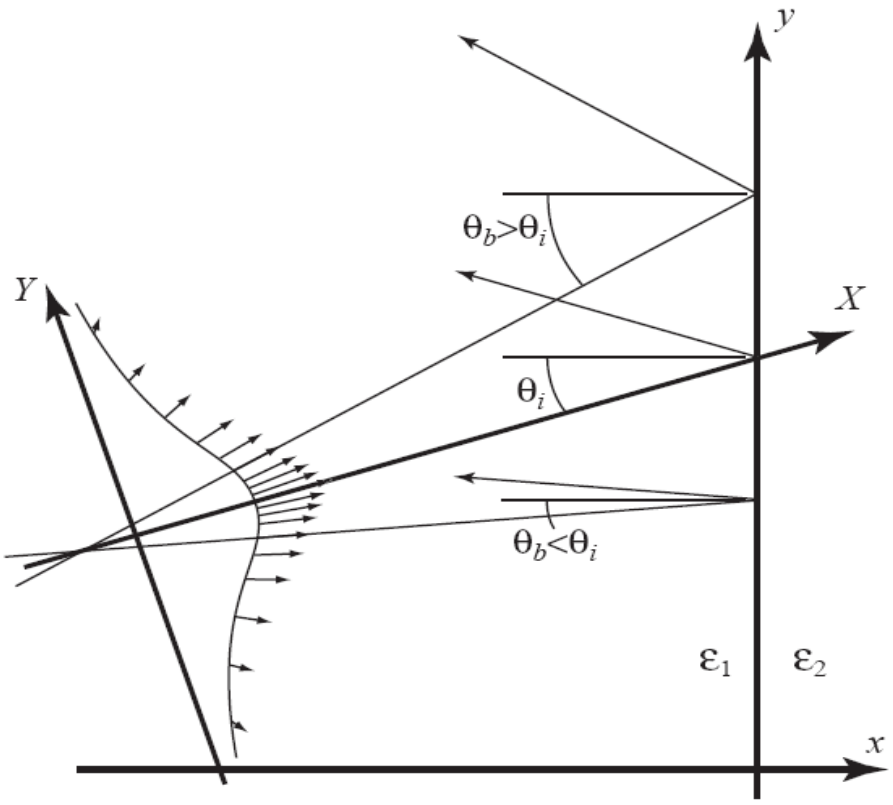

Figure 5. 8 Decomposition of an incident Gaussian beam to a spectrum of plane waves (adapted from [15] with permission from the authors).

$$E_z^i(X,Y) = \frac{1}{2\pi}\int A(k_Y)e^{-j\,k_Y Y - j\,k_X X}dk_Y\,, \tag{5.8}$$

where the amplitude of the angular spectrum is given by

$$A(k_Y) = \pi W_0^2 e^{-W_0^2 k_Y^2/4}\,, \tag{5.9}$$

and k_X and k_Y denote for the wave numbers in the X and Y direction, respectively. A component of the beam not propagating along the beam axis forms an incident angle θ_b with the x axis. The reflected beam is obtained from the incident beam spectrum but the sign of k_X changes to minus to account for the fact the reflected field propagates in the $-X$ direction and the reflection coefficient weights the angular spectrum. Because of the geometry of the FDTD simulation, the incident angle only ranges from 0 to 90 degrees. Incident and reflected power density can be

obtained from the respected fields and the square root of the ratio of these two gives the reflection coefficient.

5.4 Results of the FDTD Simulation and Theoretical Analysis

The results of both the FDTD and analytical analysis of the reflection coefficient from a gainy medium are shown in Fig. 5.9. The asterisk shows the FDTD results of the reflection coefficient of the Gaussian beam from a Lorentzian gainy medium. The open circle shows the FDTD results of the reflection coefficient of the Gaussian beam from a gainy medium where the permittivity and conductivity are constant. The dotted line shows the analytic results for the reflection coefficient obtained from a gainy medium with constant coefficients using a Gaussian beam. The

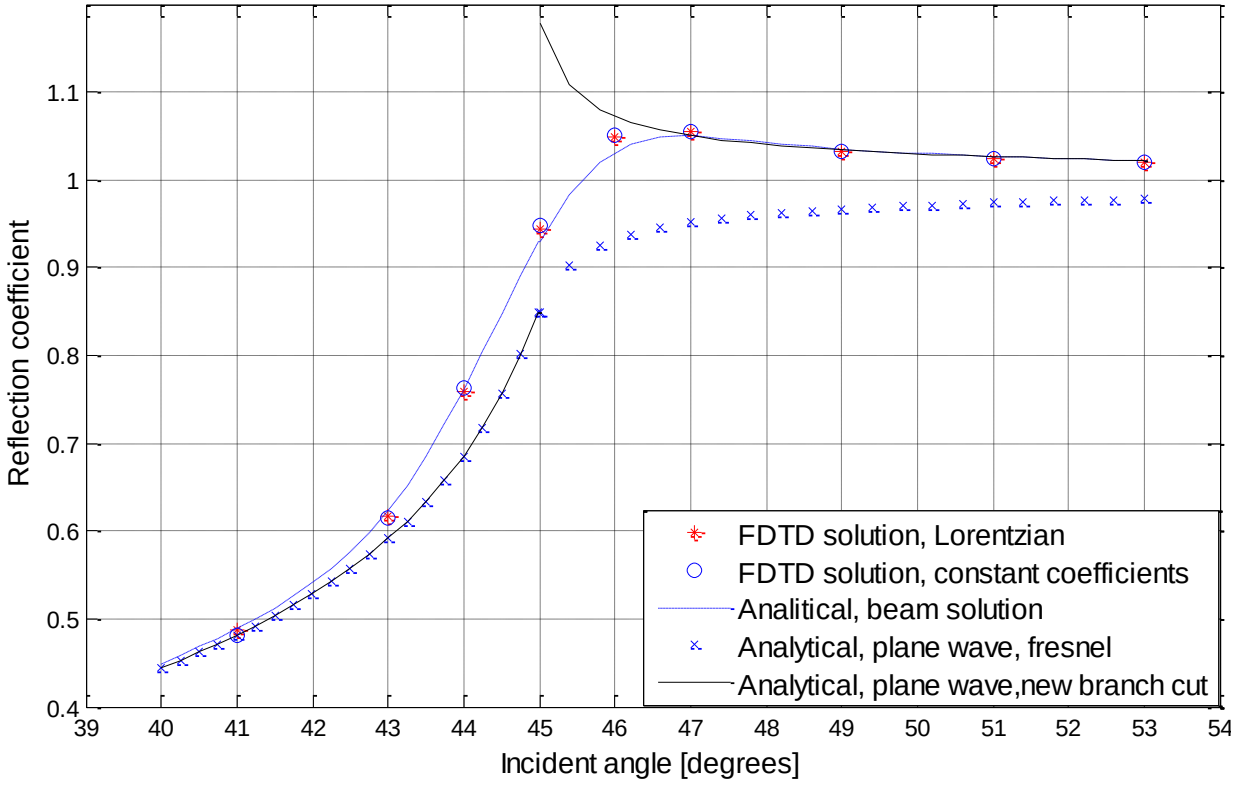

Figure 5. 9 Comparison of reflection coefficient magnitudes from a gainy medium computed for the incident beam using the analytical and FDTD method.

"x" symbol shows the analytic results for plane wave reflection from a gainy medium with constant coefficients, where we followed the traditional Fresnel equation to get the magnitude of the reflection coefficient. The line shows the analytic results for plane wave reflection from a gainy medium with constant coefficients, where we followed the new branch cut interpretation in the Fresnel equation. The reflection coefficient from the lossy media is shown in Fig. 5.10, where the interpretation of the symbols and lines are the same.

From Fig. 5.9 and Fig. 5.10, it can be seen that there is clear agreement in reflection coefficients between the FDTD results, which depends purely on Maxwell's equations, and the analytic results for beam illumination. There is a little discrepancy between the plane wave and FDTD results or beam solution, which can be attributed to the numerical approximations inherent to the FDTD formulations. The curve represented in symbol "x" in Fig. 5.9 and Fig.

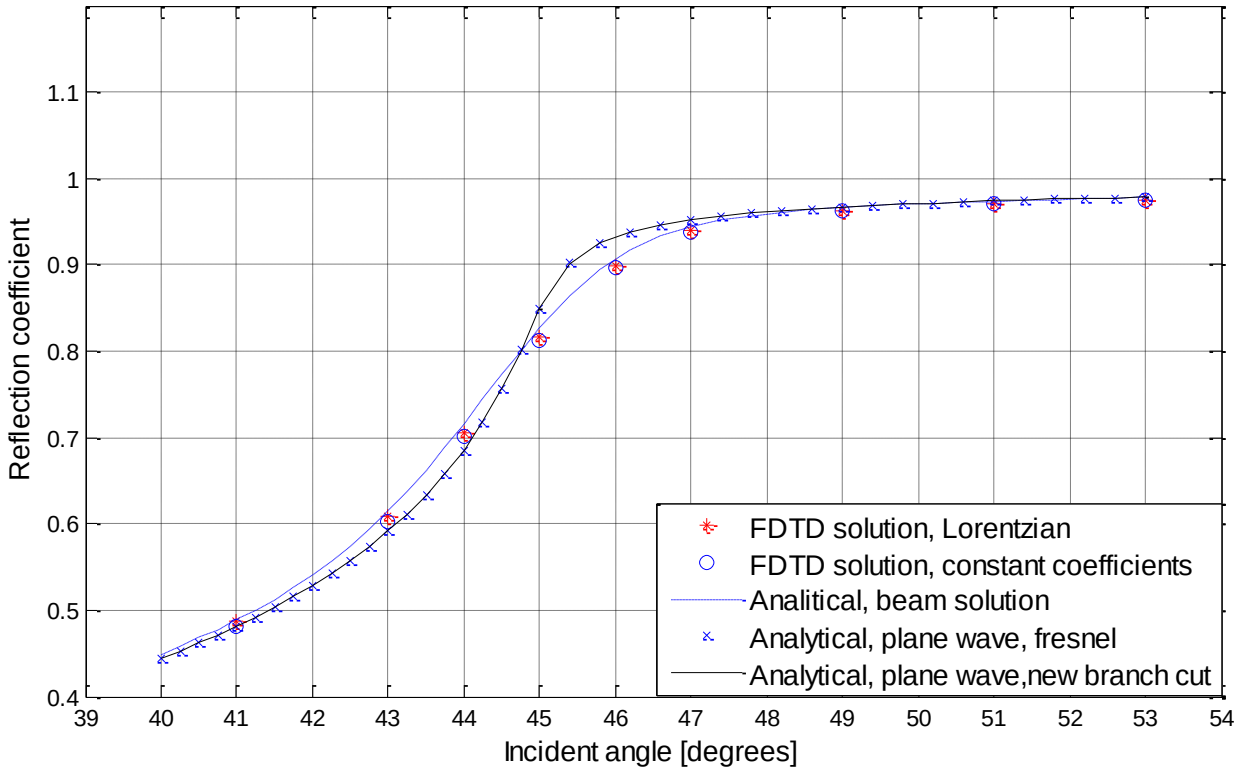

Figure 5. 10 Comparison of reflection coefficient magnitudes from lossy media computed for the incident beam using the analytical and FDTD modeling.

5.10 is the same, showing that the sign change in conductivity is not reflected in the reflection coefficient. The plane wave solution that employs the new branch cut interpretation of the Fresnel equation is affected by the sign change, and it closely agrees with the analytical and FDTD solution beyond the critical angle.

In Fig. 5.9, the plot of the analytic plane wave solution that employs the new branch cut formulation shows that the reflection coefficient is greater than unity when the incident angle is larger than the critical angle and smaller than unity when the incident angle is smaller than the critical angle. The reflection coefficient is discontinuous at the critical angle. The plots of the FDTD results for both the Lorentzian and constant coefficient materials as well as the analytic beam solution are consistent with the plane wave solution using the new branch cut, but they are continuous at the critical angle. After obtaining a maximum, all curves fall towards unity as the incident angle increases. One can also see that the reflection coefficient from a gainy Lorentzian medium at a single frequency is not distinguishable from the reflection coefficient from the medium with constant coefficients, which shows that the constant coefficient medium can serve as an approximattion for the Lorentzian materials at a single frequency in FDTD modeling for reflection problems.

5.5 Conclusion

We have conducted rigorous FDTD simulations of the interaction of a pulsed Gaussian beam with a Lorentzian or constant coefficient gainy (or lossy) half space. The FDTD computed reflection coefficient for the beam is compared to the analytically derived reflection coefficient. The results showed that there is no clear discrepancy between the reflection coefficients from a gainy (or lossy) Lorentzian half space with a gainy (or lossy) half space of constant coefficient. The magnitude of the reflection coefficient from a gainy medium will be larger than unity for

incidence above the critical angle and smaller than unity for incidence blow the critical angle. The FDTD results also confirmed the new non-conventional branch cut [15] in the complex plane defined by the critical angle.

REFERENCES

[1] Koester, C. J., "Laser action by enhanced total internal reflection," *IEEE Journal of Quantum Electronics*, Vol. QE-2, No. 9, Sep., 1966.

[2] Born, M., and Wolf, E., *Principles of Optics*, 2nd ed., New York: Pergamon Press, 1964.

[3] Diaz, R. E., and Alexopoulos, N. G., "An Analytic Continuation Method for the Analysis and Design of Dispersive Materials," *IEEE Transactions on Antennas and Propagation*, Vol. 45, No. 11, 1997, pp. 1602-1610.

[4] Gray, K. G., "The reflected impulse response of a Lorentz medium," *Proceedings of IEEE*, Vol. 68, No. 3,1980, pp. 408–409.

[5] Stanic, B. V., Milanovic, D. R., and Cvetic, J. M., "Pulse reflection from a lossy Lorentz medium half-space (TM polarization)," *Journal of Physics, D: Applied Physics*, Vol. 24, 1991, pp. 1245–1249.

[6] Cossmann, S. M., Rothwell, E. J., and Kempel, L. C., "Transient reflection of TM-polarized plane waves from a Lorentz-medium half-space," *Journal of the Optical Society of America*, Vol. 24, No. 3, 2007, pp. 882-887.

[7] Romanov, G. N., and Shakhidzhanov, S. S., "Amplification of electromagnetic field in total internal reflection from a region of inverted population," *Journal of Experimental and Theoretical Physics Letters*, Vol. 16, No. 5,1972, pp.298-301.

[8] Lebedev, S. A., Volkov, V. M., and Kogan, B. Y., "Value of the gain for light internally reflected from a medium with inverted population," *Optics and Spectroscopy*, Vol. 35, 1973, pp. 976–977.

[9] Callary, P. R., and Carniglia, C. K., "Internal reflection from an amplifying layer," *Journal of the Optical Society of America*, Vol. 66, No. 8,1976, pp. 775–779.

[10] Cybulski, R. F., and Carniglia, C. K., "Internal reflection from an exponential amplifying region," *Journal of the Optical Society of America*, Vol. 67, No. 12, Dec. 1977, pp. 1620-1627.

[11] Cybulski, R. F., and Silverman, M. P., "Enhanced internal reflection from an exponential amplifying region," Optics Letters, Vol. 8, No. 3, 1983, pp. 142-144.

[12] Cybulski, R. F., and Silverman, M. P., "Investigation of light amplification by enhanced internal reflection, Part I. Theoretical reflectance and transmittance of an exponentially nonuniform gain region," *Journal of the Optical Society of America*, Vol. 73, No. 12, Dec. 1983, pp. 1732-1738.

[13] Choi,H. H., Kim H. J., Noh, J., and Jhe, W., "Amplified Total Internal Reflection from a Plane Dielectric Boundary," *Journal of the Korean Physical Society*, Vol. 42, No. 1, January 2003, pp. 80-84.

[14] Fan, J., Dogariu, A., and Wang, L. J., "Amplified total internal reflection," *Optics Express*, Vol. 11, Issue 4, 2003, pp. 299–308.

[15] Willis, K. J., Schneider, J. B., and Hagness, S. C., "Amplified total internal reflection: theory, analysis and demonstration of existance via FDTD," *Optics Express*, Vol. 16, No. 3, 2008, pp. 1903-1914.

[16] Yee K. S., "Numerical solution of initial boundary value problems involving Maxwell's equations in isotropic media," *IEEE Transactions on Antennas and Propagation*, Vol. 14, 1966, pp. 302–307.

[17] Schneider, J. B., *"*Introduction to the Finite Difference Time-Domain method: FDTD in 1D*," Lecture materials for EE 535*, Chap. 3, WSU, 2007, pp. 34-35.

[18] Schneider, J. B*., "*Three-dimensional FDTD," *Lecture materials for EE 535*, Chap. 10, WSU, 2007, pp. 221.

[19] Taflove, A., and Hagness, S. C., *Computational Electrodynamics: The Finite-Time Domain-Method*, 3rd ed., Norwood, MA: Artech House, 2005, pp. 51.

[20] Sullivan, D. M., *Electromagnetic simulation using the FDTD method*, New York: IEEE Press, 2000, pp. 1, pp. 79.

[21] Taflove, A., and Brodwin, M. E., "Numerical solution of steady-state electromagnetic scattering problems using the time-dependent Maxwell's equations," *IEEE Transactions on Microwave Theory and Techniques*, Vol. MTT-23, No. 8, 1975, pp. 623-630.

[22] Taflove, A., and Hagness, S. C., *Computational Electrodynamics: The Finite-Time Domain-Method*, 3rd ed., Norwood, MA: Artech House, 2005, pp. 43.

[23] Merewether, D. E., Fisher, R., and Smith, F. W., "On implementing a numeric Huygen's source scheme in a finite difference program to illuminate scattering bodies," *IEEE Transactions on Nuclear. Science*, Vol. 27, No. 6, Dec. 1980, pp., 1829–1833.

[24] Mur, G., "Absorbing boundary conditions for the finite-difference approximation of the time domain electromagnetic-field equations," *IEEE Transactions on Electromagnetic Compatibility*, Vol. 23, No. 4, 1981, pp. 377-382.

[25] Umashankar, K. R., Taflove, A., "A novel method to analyze electromagnetic scattering of complex objects," *IEEE Transactions on Electromagnetic Compatibility*, Vol. EMC-24, No. 4, 1982, pp. 397-405.

[26] Schneider, J. B., and Abdijalilov, K., "Analytic field propagation TFSF boundary for FDTD problems involving planar interfaces: PECs, TE, and TM," *IEEE Transactions on Antennas and Propagation, Vol. 54, No. 9, 2006, pp. 2531-3542.*

[27] Schneider, J. B., "The TF/SF boundary for TMz polarization," *Lecture materials for EE 535*, Chap. 9.5, WSU, 2007, pp. 188-192.

[28] Taflove, A., and Hagness, S. C., *Computational Electrodynamics: The Finite-Time Domain-Method*, 3rd ed., Norwood, MA: Artech House, 2005, pp. 186.

[29] Bayliss, A., and Turkel, E., "Radiation boundary conditions for wave-like equations," *Communications on Pure and Applied Mathematics*, Vol. 23,1980, pp. 707-725.

[30] Engquist, B., Majda, A., "Absorbing boundary conditions for the numerical simulation of waves," *Mathematics of Computation*, Vol. 31,1977, pp. 629-651.

[31] Trefethen, L. N., Halpern, L., "Well-posedness of one-way wave equations and absorbing boundary conditions," *Mathematics of Computation*, Vol. 47,1986, pp. 421-435.

[32] Higdon, R. L., "Numerical absorbing boundary conditions for the wave equation," *Mathematics of Computation*, Vol. 49,1987, pp. 65-90.

[33] Liao, Z. P., Wong, H. L., Yang, B. P., Yuan, Y. F., "A transmitting boundary for transient wave analyses," *Scientia Sinica* (series A), vol. XXVII, 1984, pp. 1063-1076.

[34] Mei, K. K., Fang, J., "Superabsorption – a method to improve absorbing boundary conditions," *IEEE Transactions on Antennas and Propagation*, Vol. 40, No. 9,1992, pp. 1001-1010.

[35] Ramahi, O. M., "The complementary operators method in FDTD simulations," IEEE *Antennas and Propagation Magazine*, Vol. 39, No. 6, Dec. 1997, pp. 33-45.

[36] Ramahi, O. M., "The concurrent complementary operators method for FDTD mesh truncation," *IEEE Transactions on Antennas and Propagation*, Vol. 46,1998, pp. 1475-1482.

[37] Bérenger, J. P., "A perfectly matched layer for the absorption of electromagnetic waves," *Journal of Computational Physics*, Vol. 114,1994, pp.185-200.

[38] Schneider, J. B., "Perfectly matched layer," *Lecture Materials for EE 535*, Chap. 12, WSU, 2008, pp. 290.

[39] Taflove, A., and Hagness, S. C., *Computational Electrodynamics: The Finite-Time Domain-Method*, 3rd ed., Norwood, MA: Artech House, 2005, pp. 273.

[40] Chew, W. C., Weedon, W. H., "A 3D perfectly matched medium from modified Maxwell's equations with stretched coordinates," *IEEE Microwave and Guided Wave Letters*, Vol. 7, No. 13, 1994, pp. 599-604.

[41] Rappaport, C. M., "Perfectly matched absorbing boundary conditions based on anisotropic lossy mapping of space," *IEEE Microwave and Guided Wave Letters*, Vol. 5, No. 3, 1995, pp. 90-92.

[42] Roden J. A., and Gedney S. D., "Convolutional PML (CPML): An efficient FDTD implementation of the CFS-PML for arbitrary media," *Microwave and Optical Technology Letters*, Vol. 27, 2000, pp. 334–339.

[43] Wang, Z. Y., Zhang, Z. Q., Xu, Z. Z., and Lin, Q., "Space-time profiles of an ultra-short pulsed Gaussian beam," *IEEE Journal of Quantum Electronics*, Vol. 33, No. 4, 1997, pp. 566-573.

[44] Siegman, A. E., *Lasers*, Mill Valley, CA: Oxford University Press, 1986.

[45] Alda, J., "Laser and Gaussian Beam Propagation and Transformation," *Encyclopedia of Optical Engineering*, Ed. Johnson, R. B, and Driggers R. D., New York: Marcel Dekker, 2003, pp. 999-1013.

[46] Toll, J. S., "Causality and the dispersion relation: logical foundations," *Physical Review*, Vol. 104,1956, pp. 1760 – 1770.

[47] Jackson, J. D., *Classical Electrodynamics*, 2nd ed., New York: John Wiley & Sons,1975.

[48] Schneider, J. B., "Dispersive Material," *Lecture Material for EE 535*, Chap. 11, WSU, 2007, pp. 265-282.

[49] Kong, S. C., Simpson, J. J., and Backman, V., "ADE-FDTD scattered-field formulation for dispersive materials," *IEEE Microwave and Wireless Components Letters*, Vol.18, No.1, Jan. 2009, pp. 4-6.

[50] Taflove, A., and Hagness, S. C., *Computational Electrodynamics: The Finite-Time Domain-Method*, 3rd ed. Norwood, MA: Artech House, 2005, pp. 387-389.

[51] Robinson, D. J., and Schneider, J. B., "On the use of the geometric mean in FDTD near-to-far-field transformations," *IEEE Transactions On Antennas and Propagation*, Vol. 55, No. 11, 2007, pp. 3024-3211.

[52] Balanis, C. A., *Engineering Electromagnetics*, New York: John Wiley & Sons,1989.